TECHNISCHE UNIVERSITÄT WIEN

Master Thesis

Performance of a copper-based Oxygen Carrier for Chemical Looping Combustion of gaseous fuels

ausgeführt zum Zwecke der Erlangung des akademischen Grades eines Diplom-Ingenieurs unter der Leitung von

Univ. Prof. Dipl.-Ing. Dr.techn. Hermann Hofbauer

Projektass. Dipl.-Ing. Dr.techn. Stefan Penthor

Projektass. Dipl.-Ing. Karl Mayer

eingereicht an der Technischen Universität Wien

Fakultät für Technische Chemie

Institut für Verfahrenstechnik, Umwelttechnik und Technische Biowissenschaften

von

Jeremias Pröll, BSc

Mtr.Nr.: 0925502

Unterroith 31/10

4853 Steinbach am Attersee

Wien, September 2018

.....

Pröll Jeremias

Danksagung

Auf diesem Wege möchte ich mich kurz bei einigen Menschen für Ihr Vertrauen, Ihre Zeit und Ihre Unterstützung bedanken.

Zuallererst möchte Ich mich für die Möglichkeit der Ausführung dieser Arbeit bei Univ. Prof. Dipl.-Ing. Dr.techn. Hermann Hofbauer bedanken.

Zusätzlich gilt ein ganz besonderer Dank Dipl.-Ing. Dr.techn. Stefan Penthor und Dipl.-Ing. Karl Mayer, welche mich durchwegs optimal betreut und unterstützt haben.

Weiters bedanke ich mich bei allen Kollegen der *Zero Emission Technologies* Gruppe für eine sehr gute Zusammenarbeit und ein sehr freundliches Arbeitsklima.

Meinen Eltern gilt ein besonderer Dank für Ihren Beistand und die Ermöglichung dieses Studiums.

Meinen Geschwistern danke ich für Ihre Unterstützung wann immer Ich diese gebraucht habe.

Zu guter Letzt danke Ich meiner Lebensgefährtin, welche mich in schweren Stunden unterstützt hat und mich daraufhin immer wieder motivieren konnte.

Abstract

Chemical Looping Combustion (CLC) is a second-generation Carbon Capture. The aim of CCS is to store the separated carbon dioxide in underground deposits. The special feature of the CLC method is that the fuel and air are separated from each other. This means that there is no mixing between these gas phases. To achieve that, the required oxygen carrier is circulated between the reactors. The oxygen in the fuel reactor is obtained by the oxygen carrier. That means, that the oxygen carrier is oxidized in the air reactor, thereby the oxygen is transported to the fuel reactor, and reduced in the fuel reactor. After the reaction of the fuel with oxygen, only water vapour and carbon dioxide are produced in the fuel reactor. The water vapour is separated by a condenser and the remaining CO_2 is transported to the deposit.

In this thesis a copper based oxygen carrier, called Cu15, is analysed. This is an impregnated CuO/Al_2O_3 compound material and was tested at the *Technischen Universität Wien (TUW)* at a 120kW pilot plant. The results were compared with previous results. The 120kW system works with a Dual Circulating Fluidized Bed System.

During the experiments solid samples of the oxygen carrier were taken at each operating point. This serves to determine the oxidation state of the oxygen carrier. In addition, X-ray fluorescents analysis (XRF) and Thermo gravimetric analysis (TGA) analyses were done. The results of the investigations of the various experiments and the performance of the Cu15 oxygen carrier were discussed in this thesis. The standard conditions for the oxygen carrier were 70kW and 800°C. The fuel (natural gas) was taken from the Viennese-Gas-Grid. In addition to this fuel, higher hydrocarbons (propane, pentane) were used and analysed in various mixtures. Those fuels were passed into the fuel reactor in their gaseous phase.

All measurements of the operating points were imported, validated and optimized in the simulation program IPSEpro. Furthermore, a sensitivity analysis of small changes of the copper oxide content and the solid sample mass was presented and discussed, because of measurement errors of the oxidation state.

In general, the performance of the Cu15 oxygen carrier was good. Full conversion was achieved at higher temperatures. Higher hydrocarbons are having better combustion efficiency at lower fuel reactor specific inventories than natural gas operating points. The sensitivity analysis worked out that the influence of the parameter modification was the highest for the oxygen carrier to fuel ratio (Φ).

Kurzfassung

Chemical Looping Combustion (CLC) ist eine Carbon Capture and Storage (CCS) Technologie, welche der zweiten Generation angehört. Das Ziel der CCS Technologien ist es, dass abgetrennte Kohlendioxid in unterirdischen Lagerstätten zu speichern. Das Besondere am CLC Verfahren ist, dass der Brennstoff- und der Luftreaktor voneinander getrennt sind. Das bedeutet, dass es zu keiner Vermischung zwischen den Gasphasen kommt. Das gelingt durch den Sauerstoffträger, der zwischen den Reaktoren zirkuliert. Den Sauerstoff im Brennstoffreaktor bekommt man mithilfe des Sauerstoffträgers. Das heißt, der Sauerstoffträger wird im Luftreaktor oxidiert, dadurch wird der Sauerstoff zum Brennstoffreaktor befördert, und in diesem wird der Sauerstoffträger reduziert. Nach der Umsetzung des Brennstoffes mit Sauerstoff entsteht idealerweise nur Wasserdampf und Kohlendioxid im Brennstoffreaktor. Durch einen nachgeschalteten Kondensator wird der Wasserdampf vom CO_2 getrennt, welches dann zum Speicherort befördert wird.

In dieser Arbeit wird ein kupferbasierter Sauerstoffträger, namens Cu15 analysiert. Dieser basiert auf Kupfer und ist ein imprägniertes aus CuO/Al_2O_3 zusammengesetztes Material, das in einer 120kW Pilotanlage getestet wird. Die Resultate werden dann mit den vorherigen Ergebnissen verglichen. Die an der *Technischen Universität Wien* stehende 120kW Anlage arbeitet mit einem *Dual Circulating Fluidizied Bed* System.

Bei den durchgeführten Versuchen wurden Feststoffproben des Sauerstoffträgers bei jedem konstanten Betriebspunkt genommen. Dies dient dem Bestimmen des Oxidationszustands des Sauerstoffträgers. Zusätzlich wurden eine Röntgenfluoreszenzanalyse (XRF) und eine Thermogravimetrische Analyse (TGA) durchgeführt. Die Ergebnisse der verschiedenen Versuche und die Leistungsfähigkeit des Cu15 Sauerstoffträgers wurden in dieser Arbeit ausführlich beschrieben.

Die Standardbedingungen für den Sauerstoffträger betrugen in dieser Arbeit 70kW und 800°C. Als Standard Brennstoff (Erdgas) wurde das Gas vom Wiener-Gas-Netz genommen. Zusätzlich wurden höhere Kohlenwasserstoffe(Propan und Pentan) und Erdgas miteinander in verschieden Mixturen als Brennstoff verwendet und anschließend analysiert. Alle Brennstoffe wurden gasförmig in den Brennstoffreaktor geleitet.

Alle Messungen der konstanten Betriebspunkte sind in das Simulationsprogramm IPSEpro übertragen und validiert worden.

Weiters wurden mit einer Sensitivitätsanalyse Auswirkungen von kleinen Änderungen des Kupferoxidgehalts und der Feststoffprobenmasse dargelegt und erörtert. Dies

wurde aufgrund der aufgetretenen Probleme bei der Messung des Oxidationszustandes vorgenommen.

Im Allgemeinen war die Leistung des Cu15-Sauerstoffträgers gut. Bei höheren Temperaturen wurde eine vollständige Umwandlung erreicht. Höhere Kohlenwasserstoffe haben bei niedrigeren Brennstoffreaktor-spezifischen-Beständen eine bessere Verbrennungseffizienz als Erdgas-Betriebspunkte. Die Sensitivitätsanalyse ergab, dass der Einfluss der Parameteränderung für Φ am höchsten war.

CONTENTS

LIST OF FIGURES

LIST OF TABLES

1. INTRODUCTION

1.1 Climate Change

Barack Obama, the 44th President of the United States of America, said in his inaugural speech:

> *"[...] we will respond to the threat of climate change, knowing that the failure to do so would betray our children and future generations. [...]"* [1]

In the last four decades there have been several occurrences, which have impacted the environment and the greenhouse effect, for example the rising carbon dioxide concentration and global warming. Generally, the greenhouse effect is a natural phenomenon in the atmosphere and regulates the climate, but due to the rise in concentrations of various greenhouse gases (GHGs) such as carbon dioxide (CO_2), methane (CH_4) and nitrogen oxides the greenhouse effect is contributing more to the changes in the earth's climate.

To verify the impact of the different GHGs, they have to be measured and compared. This is enabled through the CO_2 equivalent (CO_2eq). This parameter describes how much of the mass of a GHG mixture contributes to global warming compared to the CO_2 value. The CO_2eq is calculated over a specific period of time, usually a timeframe of 100 years.

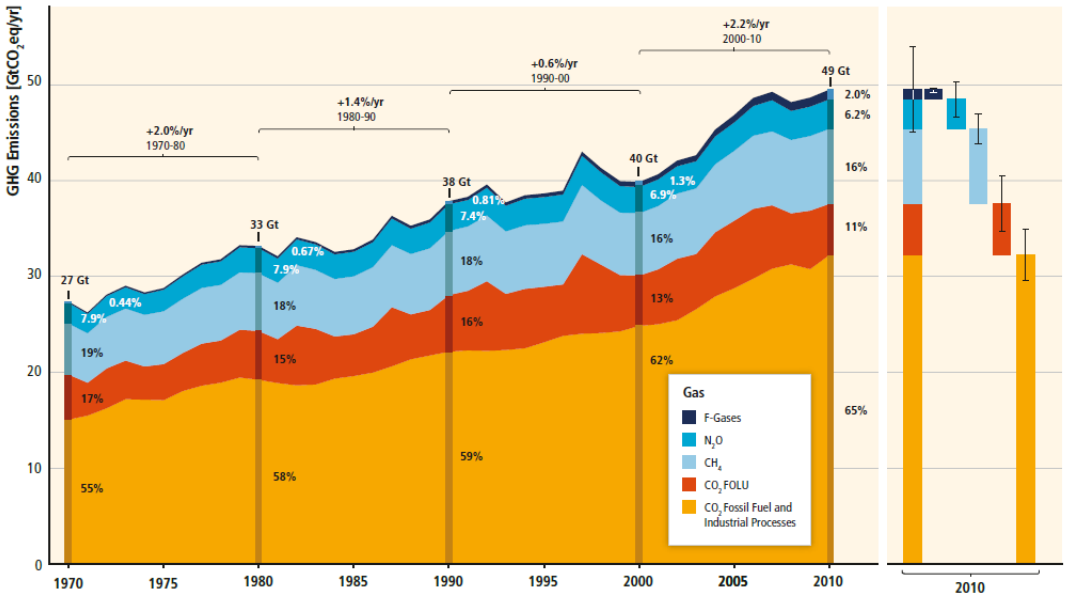

Figure 1. 1: GHG emissions between 1970-2010 (taken from [2])

These concentrations rose more between 2000 and 2010 than in the decades from 1970 to 2000. There was an increase of 2.2%/a between 2000 and 2010 whereas the increase between 1990 and 2000 was only 0.6%/a. To explain that in more detail the $GtCO_2eq/a$ emission rose from 40 to 49 $GtCO_2eq$ in the years between 2000 to 2010 (Figure 1. 1). [2]

This emission results from the sectors in Figure 1. 2:

- Electricity and Heat Production
- Industry
- Transport
- Buildings
- Agriculture, Forestry and Other Land Use (AFOLU)
- Other Energy

Generally global warming is a naturally occurring phenomenon, but normally takes place at a much slower rate, a rate that has now been shown to be increased by many man-made sectors. The sectors in the following chart have had the greatest impact on the GHG emission and on the environment. [2]

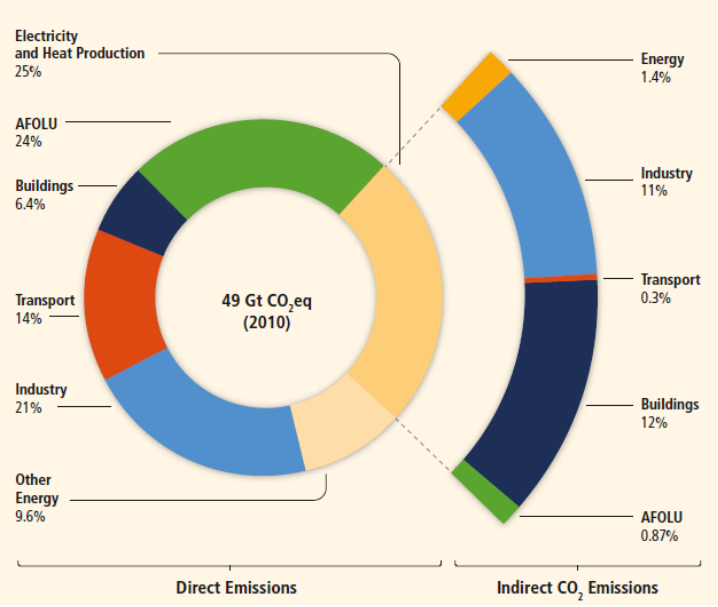

Figure 1. 2: GHG emissions divided into sectors (taken from [2])

The consequences of the increasing rate of the greenhouse effect are mainly the irreversible changes to the environment and the climate. The *Royal Society* and the *US*

National Academy of Science reveal in Figure 1. 3 that the global average air surface temperature has increased by 0.8°C since 1900. [3]

The described increase of the temperature in Figure 1. 3 refers to the climate, not to the weather. To make that clear there is a difference between climate and weather. Climate refers to the average of the weather over a specific period of time, whereas the weather itself is the state of various measurable parameters such as humidity, temperature and pressure at a specific moment and a specific place.

The earth's climate can be divided in several spheres. The five spheres are called atmosphere, hydrosphere, cryosphere, lithosphere and biosphere. These spheres together are a natural system which is boosted by the energy of the sun. The system gets disrupted by the GHGs, because of their influence on the radiation in the atmosphere. This radiation naturally comes from the sun and therefore the GHGs are responsible for reflecting the radiation back to the Earth's surface and the absorption of the radiated by the atmosphere. The consequence of this is global warming. [4]

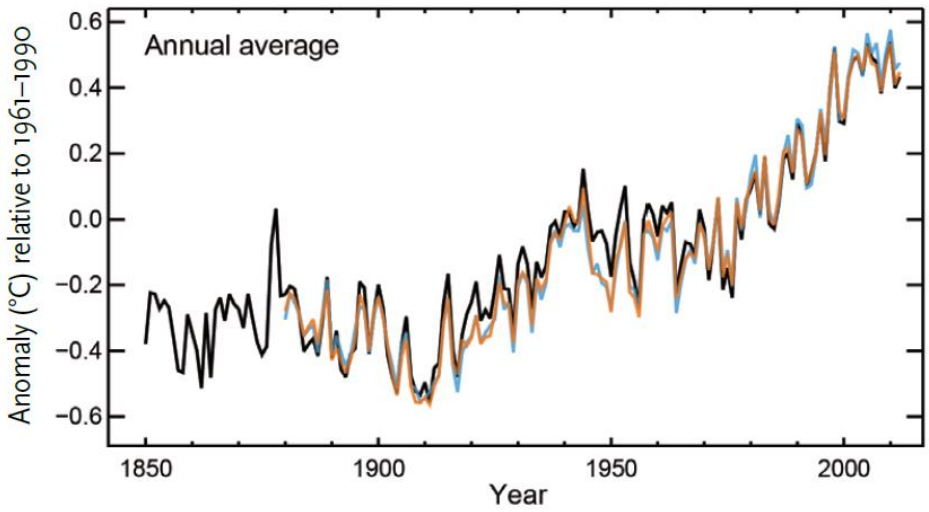

Figure 1. 3: Average temperature since 1850 (taken from [3])

The most noticeable effects of the observed increase of the temperature are: [3] [4]

- The glaciers retreat
  Due to the increasing temperatures, the glaciers mass has decreased over the last decades.
- Shrinking of the arctic sea ice
  The arctic ice has decreased because of global warming during the last decades.

- The rise of the sea level
  The increasing sea level is a consequence of glacial retreat and the melting arctic sea ice.

- Many animals are endangered by current weather conditions like extremely hot summers and unnaturally cold winters. Therefore, they have to find new habitats.

Many of the problems that have arisen due to global warming are therefore directly linked to the growing CO_2 concentration in the atmosphere. [4]

1.2 Scenarios to reduce CO_2 Emissions

The different scenarios of representative concentration pathways (RCP) were depicted in patterns by the Intergovernmental Panel on Climate Change (IPCC). These are climate predictions and projections patterns which show an increase of CO_2eq from 430ppm to over 1000ppm in the year of 2100. The patterns are called RCP2.6, RCP4.5, RCP6.0 and RCP8.5. They are named after the range of the radiative forcing in 2100 compared to the preindustrial values. [2]

The different scenarios are shown in Figure 1. 4**:**

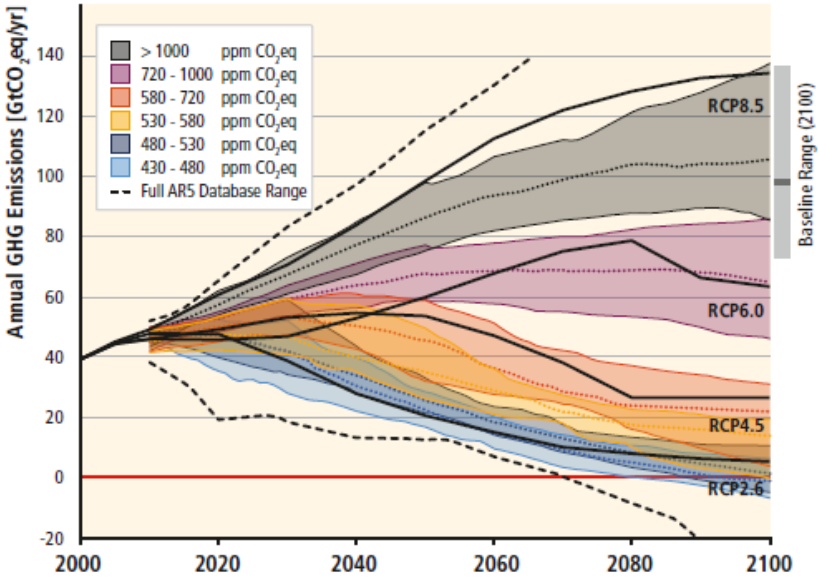

Figure 1. 4: Total GHG emission in all AR5 scenarios (taken from [2])

RCP2.6: In this scenario the CO_2 emissions are reduced and the peak of the radiative force is at 3W/m^2. In the year 2100 the radiation energy will be 2.6W/m² and will

decrease after the year 2100. The CO_2 concentration in the aerosphere will be 450ppm CO_2eq in the same year.

RCP4.5, RCP6.0: In those intermediate scenarios the radiation energy will stabilize at 4.5 and 6.0W/m^2 after 2100. The reduction of the GHGs emissions will start in 2040 for the RCP4.5 and in 2080 for the RCP6.0. The RCP6.0 pattern shows that the CO_2 concentration in the aerosphere will be 720-1000ppmCO_2eq whereas the CO_2 concentration in the aerosphere in pattern RCP4.5 will be 580-720ppmCO_2eq.

RCP8.5: In this scenario the radiative force reaches more than 8.5W/m^2 until the year 2100 and continues to show further increases. Therefore, the emissions are increasing as usual. The CO_2 concentration in the aerosphere will be higher than 1000ppmCO_2eq in 2100.

The change of temperature can only be below the calculated temperature of 2°C, if the concentration does not reach over 450ppmCO_2eq in 2100. The planned target to stay under 2°C cannot be reached if the concentration really reaches 650ppmCO_2eq in 2100. Therefore, the RCP2.6 is the only one that could achieve this result of 2°C. To stay under 3°C the concentration must not exceed 650ppmCO_2eq and to stay under 4°C the concentration must not exceed 1000ppmCO_2eq. [2]

1.3 Technologies to reduce CO_2 Emission

To reduce the greenhouse effect a decrease of GHG emissions is essential. The five different scenarios of the IPCC are shown in Figure 1. 4. Measures must be set and a variety of technologies have to be used to stay under the planned target of the increasing 2°C. This target was reinforced by the United Nations Framework Convention on Climate Change (UNFCCC) in 2015 in Paris. It became applicable on 4.Nov 2016, when 55% of the emission causing states and minimum 55 states ratify the agreement.

Figure 1. 5 gives an impression of how it could look in 2050, if the technologies are used and the measures are implemented. This figure shows the most efficient economic way to reduce the CO_2 emissions. To reach this economic goal different technologies are used. The use of renewable technologies like wind power, hydropower or the use of biomass instead of fossil fuels is one part in this scenario. Furthermore, a reduction of GHG emissions can be also reached through an increase of the end use of power and electricity efficiency and with an increased use of nuclear power. Carbon Capture and Storage (CCS) can also reduce CO_2 emissions. The aim of

CCS is to store the GHG, especially CO_2 in the subsurface. All these points which are mentioned are necessary to reach this economic goal by 2050. [5]

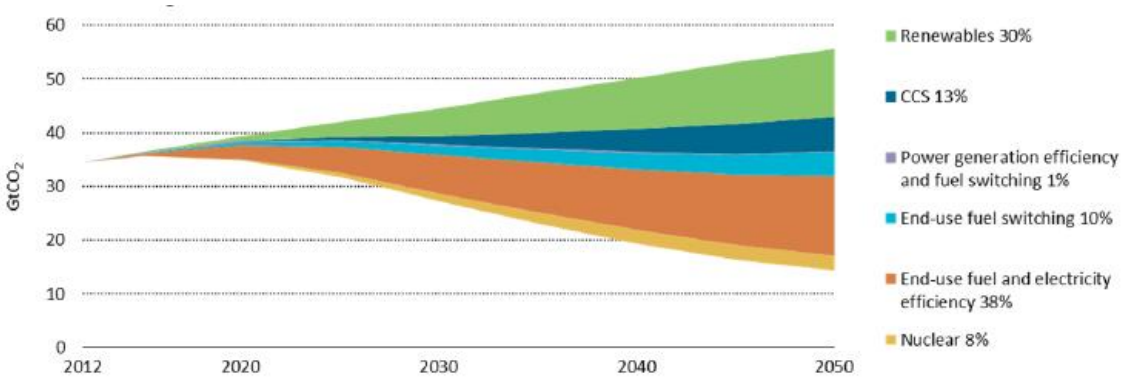

Figure 1. 5: Technology outlook until 2050 (taken from [5])

1.4 Carbon Capture and Storage

1.4.1 Rationale for Carbon Capture and Storage

Carbon Capture and Storage is one of the proposed solutions to reduce CO_2 emissions. CCS may be able to contribute to a reduction of carbon dioxide emissions of up to 13% by 2050 (Figure 1. 5). The CO_2 can be separated before or after combustion. Once it is separated, the CO_2 can be stored underground. As a consequence, fossil fuels can be used without the danger of increasing the levels of CO_2 emitted into the atmosphere.

The use of fossil fuels will not be reduced so quickly. That is because industrial countries still rely heavily on fossil fuels. By far the two largest energy consumers are the United States of America and China. Their use of coal, natural gas and petroleum is significantly higher than the fossil fuel consumption of the rest of the world. The International Energy Agency (IEA) assumes that at least 80% of CCS is increasingly used in these two countries.

The possibilities and applications of CCS technologies are widespread [5]:

- CCS applied on gas fired power units is especially useful when the gas prices are low. That can be effectively implemented in the USA for example.
- Another application is natural gas processing where the natural gas stream can be separated from the CO_2 before it is sold. It is a method in the *Australian Gorgon Project*.

- In industrial sectors like cement or steel production a reduction of CO_2 emissions is also possible, a good example is the *Abu Dhabi CCS project*.
- CCS applied to energy production through coal; in 2014 the first commercial CCS application starts to work at *Sask Power's Boundary Dam Station*.
- The bio-energy with CCS (BECCS) is using biomass for the combustion process and stores the CO_2 afterwards. Therefore a "negative emission" is possible. That is because the biomass removes atmospheric carbon.
- The Enhanced Oil Recovery using CO_2 (EOR) is a method to store the CO_2 in already developed oil fields. The gas is pumped down to release the remaining oil in the formations. This method is also used in the *Abu Dhabi CCS project.*

Another method of achieving a reduction of atmospheric CO_2 emissions is Carbon capture and utilisation (CCU). The difference between CCU and CCS is that the CO_2 is used as a resource and not stored underground. The EOR which is mentioned before is one example for using CO_2. Another possibility is direct utilisation of CO_2, for example as carbonating argent in the food and drinks industries or in the pharmaceutical industry as a respiratory stimulant. But CO_2 can also be used for the production of fuels like it is in Fischer - Tropsch Synthesis. In other chemical processes CO_2 reacts with metal oxides to form carbonates. The cultivation of algae and their use as a bio fuel is also another possibility. The advantage is that algae can breakdown CO_2 directly from exhaust gas streams (Figure 1. 6). [6]

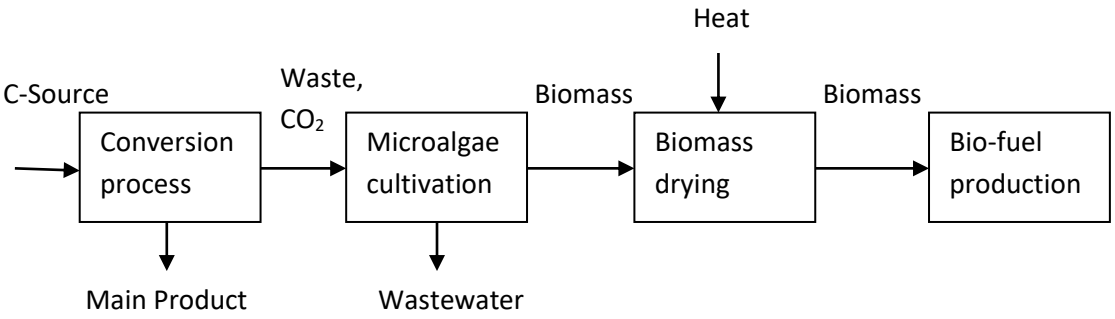

Figure 1. 6: CCU: production of bio-fuels from Algae

1.4.2 Carbon Capture and Storage

The aim of CCS is to store the captured CO_2 underground, to prevent its release into the atmosphere. Therefore, CCS can be divided into three steps. The first one is to capture the CO_2 and separate it from other flue gases. The second step is to transport the CO_2 to the storage. The third one is to store it underground. [6]

To describe the capture of CO_2 in more detail, the technologies can be divided in four groups. The target of all four groups is to produce very highly concentrated CO_2 streams.

The Post Combustion Capture Technology (Figure 1. 7) leads to a separation of CO_2 out of the flue gas stream by adsorption or absorption. This separation happens after combustion, where the carbon source produces the CO_2. Fossil fuels are an example of carbon sources. The Post Combustion Technology can be applied to existing power units like those used in cement, fuel and steel production. [6]

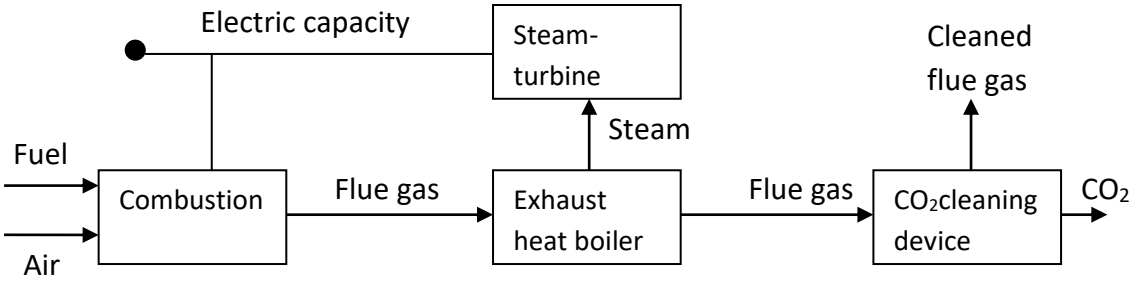

Figure 1. 7: Schema of the Post Combustion Capture Technology

In *the Pre Combustion Capture Technology* (Figure 1. 8) the CO_2 is separated from the fuel before the combustion happens. That starts with the conversion of the carbon source into synthesis gas (syngas). Syngas is defined as H_2, CO and CO_2. The syngas reacts through the water gas shift reaction with water to H_2 and CO_2. Afterwards the CO_2 can be removed from the H_2, which is used as fuel for combustion. [7]

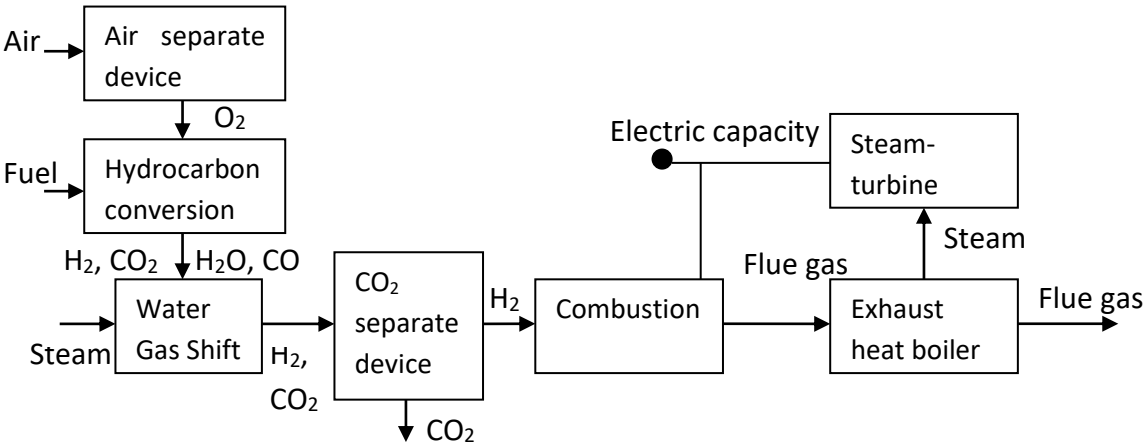

Figure 1. 8: Schema of the Pre Combustion Capture Technology

In the *Oxyfuel Technology* oxygen (O_2) gets separated by an air separation unit, to obtain pure oxygen. Afterwards the O_2 is mixed with the fuel for combustion. The big advantage of this technology is that the flue gas stream has mostly combustion products and no nitrogen from air. The water in the exhaust gas stream gets separated from the CO_2 through a condenser. [7]

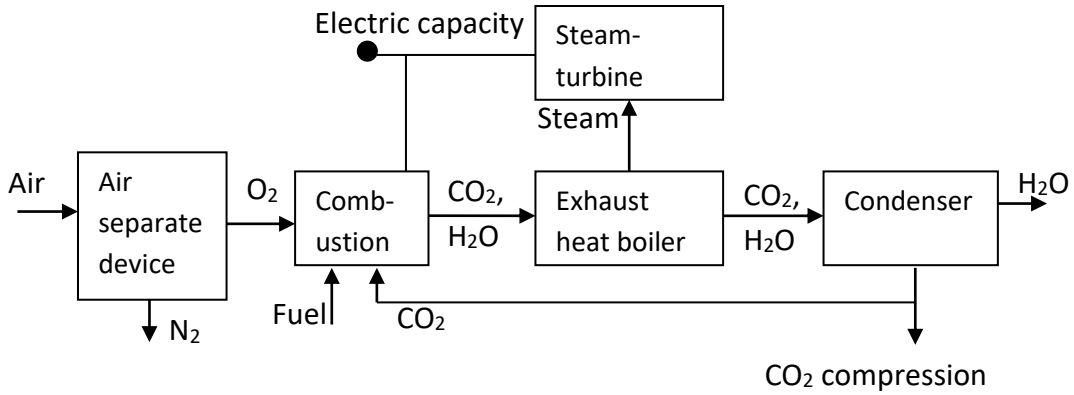

Figure 1. 9: Schema of the Oxyfuel technology

The main difference to the other technologies is that, in *Unmixed Combustion*, oxygen is chemical bonded to catalysts. These catalysts, e.g. metal oxides, can store the oxygen from the air and lead it to the fuel. Therefore, the metal oxides are oxidized and reduced. In ideal conditions the exhaust gas stream consists only of H_2O and CO_2 after combustion. Those two components can be separated by using a condenser afterwards. Chemical looping combustion (CLC) is an example of unmixed combustion. [7]

There are two possible ways to transport the CO_2. The first one is through the use of pipelines, whereas the second one is to ship the CO_2 to the storage facility. The advantage of transporting the CO_2 by ship is that the ship can transport the CO_2 for a longer distance. Examples of possible storage facilities for the CO_2 are depleted gas or oil fields, not recoverable coal reserves or saline aquifers. To store the CO_2 in the deep sea is less pursued because of possible unknown environmental damages. [8]

1.4.3 Chemical Looping Combustion

In the CLC technology air and fuel are never mixed. The CLC process has two steps. The first one is the oxidation of the oxygen carrier (OC) with air in the air reactor (AR). An oxygen carrier is a solid catalyst like a metal oxide which transports the oxygen from the air reactor to the fuel reactor (FR). The second one is the reduction of the oxygen

carrier in the fuel reactor, where the fuel gets oxidized through contact with the OC. The advantage is that the exhaust gas streams of both reactors never get mixed. This results in an exhaust gas stream that ideally consists of steam and CO_2 after the fuel reactor. After passing through the air reactor, the exhaust gas stream consists of depleted air. Therefore, the fuel reactor exhaust gas can be separated with a condenser. The energy intensive gas-gas separation is missing and therefore raises the efficiency of the whole process. [4]

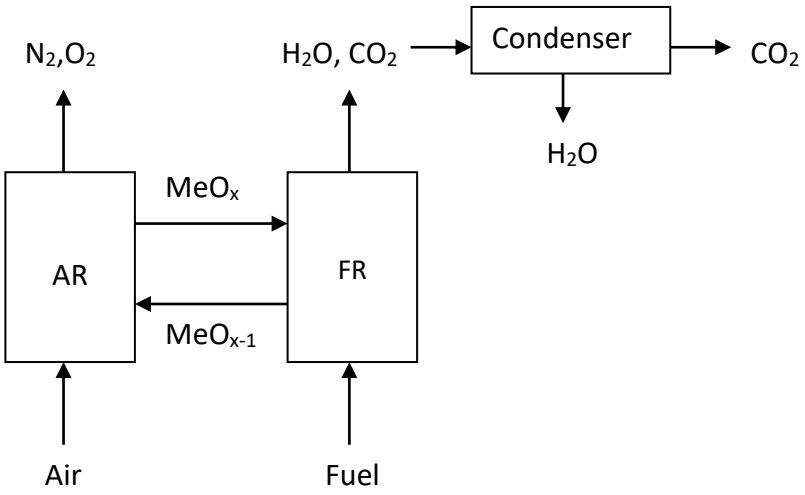

Figure 1. 10: Schema of the chemical looping process

Figure 1. 10 shows the schema of the CLC process. Fluidised beds are mostly used in these reactor concepts. The AR is fluidised with air whereas the FR is fluidised with the fuel itself in the case of gashouse fuels. As a carbon source, different fuels can be used, such as natural gas, propane or pentane. As bed material for the fluidised beds, the OC is used. Those are mostly compound materials of metal oxides with inert materials.

1.5 Motivation and Objectives

The objective of this present work is the investigation of a copper OC material called Cu15. This is an impregnated CuO/Al_2O_3 compound material. The experiments were performed at the 120kW chemical looping pilot plant at *Technische Universität Wien (TUW)*.

The experiments and subsequent analysis are discussed and explained.

Specific Objectives were determination of:

- the performance of the Cu15- OC: fuel conversion behaviour
- the process performance of Cu15 with higher hydrocarbons
- the analysis of possible errors of the oxidation state of the solid sample when using a reduction furnace and a muffle furnace
- a sensitivity analysis regarding influence of measurement errors on process parameters

2. THEORETICAL BACKGROUND

2.1 Fluidized Bed Technology

Generally, two phases are involved in the fluidized bed technology: a solid and a fluid phase. The solid phase is a stationary bed of solid particles. A fluid is flowed through this phase. If the velocity of the fluid is high enough, the particles begin to move, so that individual particles are placed in a floating state. After that velocity has been reached the state is called the fluidization. As a result of the contact between the solid and fluid phase, heat and mass transport processes are favoured.

The differences between a fixed and a fluidized bed can be described in a pressure loss diagram. On the x-axis the velocity is plotted and on the y-axis the pressure loss. It shows that the pressure loss is rising with the increasing velocity until the minimum fluidization velocity has been reached. After this point, the pressure loss is stagnant and a fluidized bed is built. When the velocity is further rising and is higher than the sedimentation velocity of the particles, the pressure loss is rising again and the particles will fall out. This is called pneumatic transport. Figure 2. 1 shows those coherences. [9]

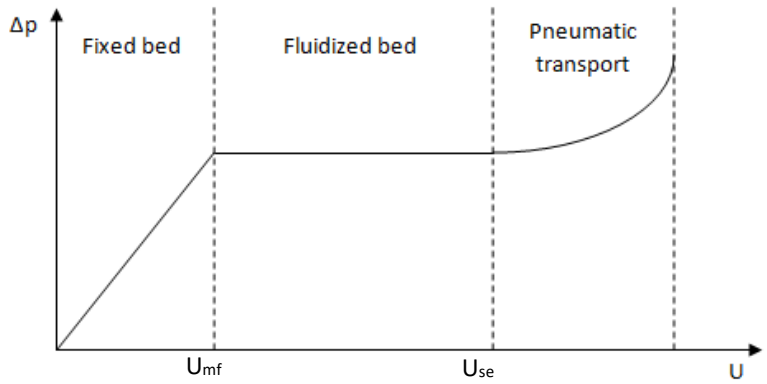

Figure 2. 1: Range of fluidized bed with increasing velocity and pressure loss (taken from [9])

2.1.1 Geldart Particle Classification

D. Geldart characterized the behaviour of particles in fluidized beds. He split the particles into four groups. The distinction between them is the density and the particle size. This is shown in Figure 2. 2.

Generally, there are four groups [10]:

- Group A: They exhibit very low cohesion and a small size.
  - E.g.: Typically, catalysts
- Group B: Material with medium size, which build fast bubbles.
  - E.g.: Sand
- Group C: These particles are very fine materials which are strongly cohesive.
  - E.g.: Flour or cement
- Group D: Very big particles or particles with higher density.
  - E.g.: Coffee beans

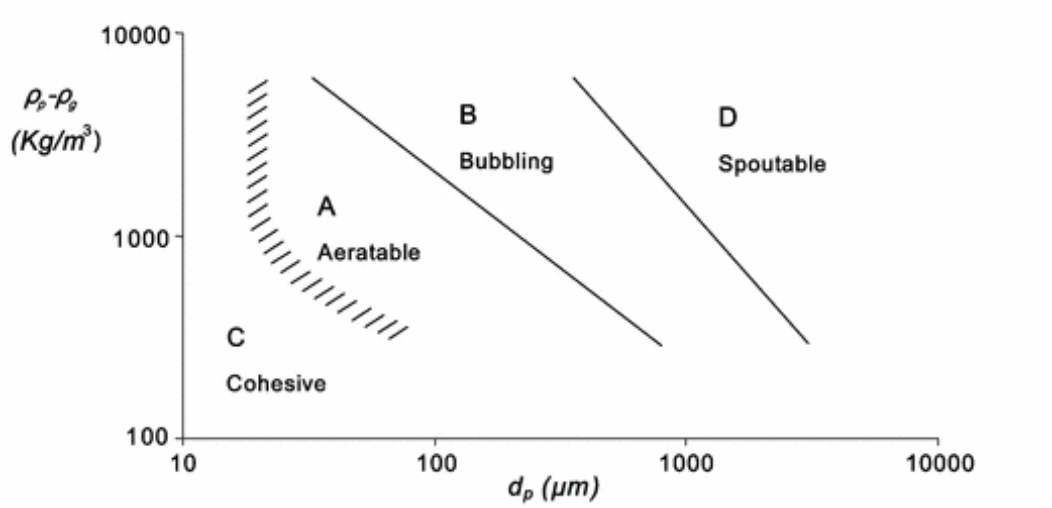

Figure 2. 2: Classification according to *D. Geldart* (taken from [11])

2.1.2 Fluidization Regimes of Solid Materials

The different fluidization regimes are introduced in a diagram by *L. Reh.* In this diagram, the fluidization regimes are described with the help of dimensionless numbers. Those are the *Reynolds-number (Re), the Archimedes-number (Ar), the Froude-number (Fr) and the Ω-number.* The regimes are: the fixed bed, the fluidized bed, circulating fluidized bed and the solids discharge.

J.R. Grace combined the ideas of D. *Geldart* and L. *Reh* and introduced the dimensionless numbers d_p^* and U^*. With these dimensionless numbers, the different groups and the fluidization regime are described in the Grace diagram (Figure 2. 3).

$$d_p^* = Ar^{1/3} = d_p \left[\frac{\rho_g g \Delta\rho}{\mu^2}\right]^{1/3} \quad (1)$$

$$U^* = Re/Ar^{1/3} = U \left[\frac{\rho_g^2}{\mu g \Delta\rho}\right]^{1/3} \quad (2)$$

The equations above describe the dimensionless numbers of the *Grace* diagram below (Figure 2. 3). The particle diameters as well as the gas velocity are dimensionless. The particle diameter d_p^* includes *Ar*, which contains the ratio of the buoyancy force to frictional force. U^* is the gas velocity which is the ratio of the dimensionless numbers of *Re* to *Ar*. This velocity is flowed through the solid bed. The Re number describes the ratio of the inert force to the dynamic or kinematic viscous force. So U^* characterises both dimensionless numbers, *Re* and *Ar*.

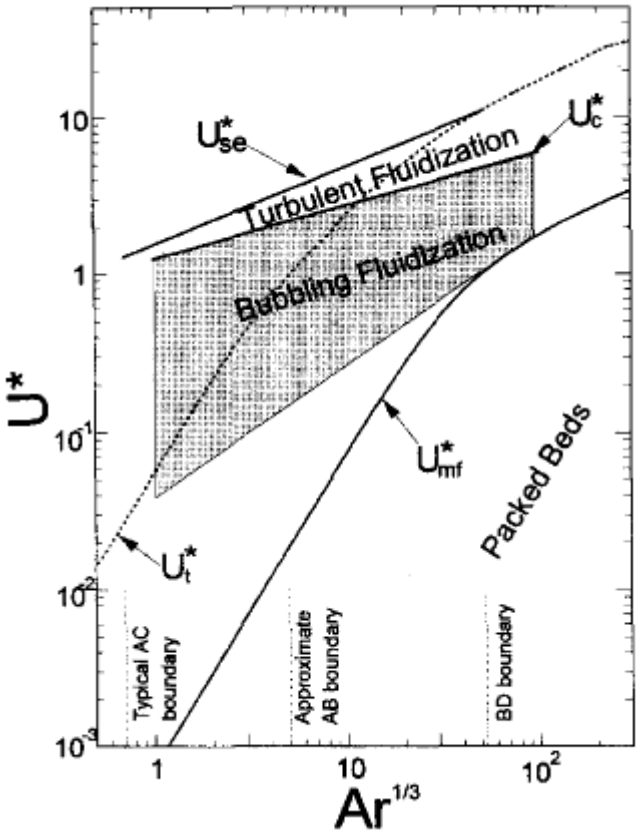

Figure 2. 3: Gas solid fluidization diagram according to *Grace* (taken from [12])

Table 2. 1 illustrates that there are different velocities to describe the fluidization regime. Besides that, the different particle groups, which were described before, are connected in the *Grace* diagram (Figure 2. 3). It shows that the regimes are separated by specified velocities. U_{mf}^* is the minimum fluidization velocity, below that the solid

phase is a packed bed, where the gas stream is moving through the intermediate spaces of the solid bed. Only when the minimum fluidization velocity, U_{mf}^*, is reached it is a fluidized bed, if not it is a fixed bed.

The bubbling bed is characterised for building gas bubbles which lead to a better intermixing. Those different regimes are illustrated in Figure 2. 4. If the velocity is further increased the bed will expand and after the critical gas velocity, U_c^*, is reached, the regime is a turbulent fluidized bed. Between U_c^* and U_{se}^* there is a turbulent behaviour.

The solid entrainment velocity, U_{se}^*, is the point where particles cannot be held in the system, therefore a recirculation can be used to prevent that the particles flow out of the system. The two regimes where the velocity is higher than U_{se} are called fast fluidization and pneumatic transport. At the fast fluidization regime, the particles are moving with the gas stream in the middle of the reactor up and near to the wall, as particle clusters, they are moving down. At the pneumatic transport the solid concentration in the reactor is very low and the same everywhere, except at the bottom. [12] [9] [13]

Table 2. 1: Different fluidization regimes with increasing velocity (taken from [13])

FLUIDIZATION SYSTEMS	VELOCITY RANGE	DESCRIPTION
FIXED BED	$0<U<U_{mf}$	The velocity is too small to reach the point where pack expands. The pressure loss is rising.
BUBBLING	$U_{mb}<U<U_c$	The minimum bubbling velocity is reached. A better intermixing is the consequence.
TURBULENT	$U_c<U_{se}$	Characteristically the maximum pressure loss takes place and the first particle falls out. Sometimes packages of particles occur.
FAST FLUIDIZATION	$U>U_{se}$	A lot more particles are lost and there is no more homogeny distribution.
PNEUMATIC TRANSPORT	$U>>U_{se}$	The velocity is much higher than in the fast fluidization and a lot more particles fall out.

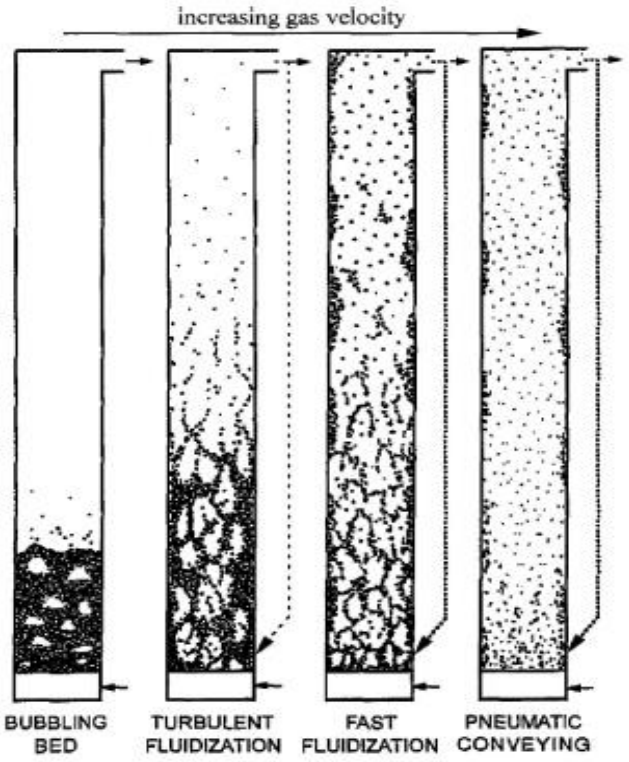

Figure 2. 4: Fluidized bed regimes. (taken from [14])

2.2 Chemical looping Combustion

In the previous section 1.4.3 CLC is described in an overview. This chapter further describes thermodynamics and the reactor system while giving more information about oxygen carriers, especially the Cu15 oxygen carrier.

In 1954, *E. Gilliland* and *W*. *Lewis* invented the design of a facility, which produces pure CO_2. [15] After this invention, it took 40 years until it was used for Carbon Capture and Storage which was the idea of *M. Ishida, D. Theng* and *T. Akehata* in 1987.

2.2.1 Process Objectives

The process objectives have to be fulfilled to get a viable result with respect to the environment and the economics. The key facts and goals of the objectives have to be mentioned: A good fuel conversion is the foundation of using CLC. Additionally, a deactivation, for example by coke, of the OC has to be prevented. The fluidized bed ability of the OC has to be provided and the attrition of the OC has to be minimalised. The OC should be non-toxic and environmentally and economically sustainable. [16] [4]

To explain the process in more detail the **general reactions** are important: [14] [17] [18]

Fuel reactor:

The goal of the FR is to achieve full conversion of the fuel. The fuel can be natural gas, higher hydrocarbons, syngas or solid fuels, like biomass. In this master thesis, natural gas and higher hydrocarbons are used as fuel.

The main reaction in the FR:

$$(2n+m)MeO_a + C_nH_{2m} \rightarrow (2n+m)MeO_{a-1} + mH_2O + nCO_2 \quad (3)$$

That includes:

$$C_xH_y + xMeO_a \rightarrow xCO + \frac{y}{2}H_2 + xMeO_{a-1} \quad (4)$$

$$CO + MeO_a \leftrightarrow CO_2 + MeO_{a-1} \quad (5)$$

$$H_2 + MeO_a \leftrightarrow H_2O + MeO_{a-1} \quad (6)$$

Air reactor:

With the reaction below the OC is oxidized again:

$$MeO_{a-1} + \frac{1}{2}O_2 \rightarrow MeO_a \quad (7)$$

Water gas shift reaction:

This reaction occurs mostly with the steam reforming reaction, where the carbon monoxide is produced.

$$CO + H_2O \leftrightarrow CO_2 + H_2 \quad (8)$$

Steam reforming reaction:

Steam reforming is a reaction that produces carbon monoxide and hydrogen. This reaction is exothermic whereas the water gas shift reaction is endothermic.

$$C_xH_y + H_2O \leftrightarrow CO + \left(x + \frac{y}{2}\right)H_2 \quad (9)$$

Chemical looping with oxygen uncoupling: [19]

The goal of chemical looping with oxygen uncoupling (CLOU) is to release gaseous oxygen in the FR. During the combustion, CLOU allows an inherent separation of CO_2 of different fuels. These can be solid or gaseous fuels. Therefore, the OC must be able to release the gaseous oxygen under suitable thermal conditions in the FR. The fuel reacts afterwards with the gaseous oxygen in the FR to CO_2 and H_2O. The oxidation of the OC happens in the AR and is transported to the FR, where the OC gets reduced. Therefore, the OC has to be able to capture, in the AR, and release gaseous oxygen, in the FR.

$$Me_xO_y \rightarrow Me_xO_{y-2} + O_2 \tag{10}$$

$$C_xH_y + \left(x + \frac{y}{2}\right) O_2 \rightarrow xCO_2 + \frac{y}{2} H_2O \tag{11}$$

2.2.2 Oxygen Carrier

Oxygen carriers are metal oxides and are coupled with an inert material. In previous works various OCs were described. The OCs can be separated in two main groups of OC. The first group consists of natural ores; natural ilmenite is an example of a natural ore OC. The second group is made up of the synthetic OC. Those are based on materials like Cu, Fe, Mn and Ni and they are produced using different methods, for example by spray-drying or impregnation. To verify a substance will be effective as an OC it has to display certain important characteristics. These are generally: a high reactivity of an OC, a high oxygen transport capacity, high mechanical strength and low production costs. Therefore, an OC with lower costs of production and raw material can be more viable than an expensive one. This is because the lower costs compensate for the lower life time. Cheaper OCs are mostly natural ores. On the other hand, a longer lifetime can compensate for high production costs. The balance of the production costs and the lifetime is a matter that cannot be ignored. It is not only the costs of the material itself that are relevant for fuel conversion. The thermodynamics, the reactivity of the OC and its oxygen transport capacity are parameters which also decide how much material has to be used for the conversion of the fuel. [4][26]

The synthetic OC are synthesised from pure chemicals. The core is mostly an inert material and is impregnated by the OC. This leads to better OC characteristics, like thermal stability, low abrasion or high porosity. [20]

Redox potential and equilibrium of OC:

Generally, two reaction partners react with each other. One of them gets oxidized and the other gets reduced. The redox potential is the sum of the oxidation and reduction potential of the two partners. The equilibrium ratio of CO/CO_2 and H_2/H_2O of different OC shows the possibility of full fuel conversion in the CLC process. Therefore, the H_2 and CO reaction must be fulfilled. That means that no CO and H_2 is in the FR after the combustion. Figure 2. 5 shows the different equilibrium - ratios of different oxygen carriers at 850°C. It shows that the Cu equilibrium ratio is the lowest and the Ni equilibrium ratio is the highest. This demonstrates the fact that Cu has no limitation of full fuel conversion. It has to be mentioned that not only the thermodynamics but also the reactivity of the OC is an important factor for the CLC process. Therefore, while the Ni-based OC has a good operating performance, it does not display the best equilibrium. [14] [4] [21]

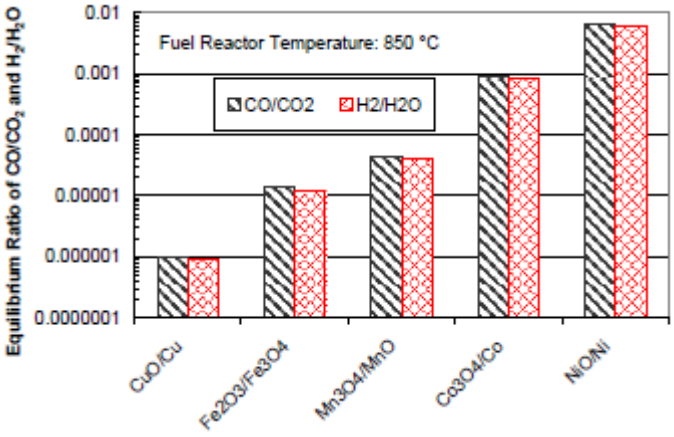

Figure 2. 5: Equilibrium of different OC (taken from [14])

2.2.3 Copper based OC and the Cu15 oxygen carrier

The Cu15 is a copper based OC which is coupled with an inert material, Al_2O_3. It is prepared by impregnation using Al_2O_3 as support material. Other inert materials such as SiO or $MgAl_2O_4$ can be used; however, the advantage of a copper-based oxygen carrier is that they theoretically fully convert the complete fuel to carbon dioxide and steam (Figure 2. 5). A negative aspect is that copper based oxygen carriers have a low melting point and higher cost when compared to an OC like Mn or Fe. Different experiments and research have been done with copper based OC. *Adanez et al.* [22] operated at a 10KW unit with a $CuO\text{-}Al_2O_3$ OC. The result is that a full conversion of methane took place at a temperature of about 800°C and that the OC-to-fuel-ratio (Φ)

was higher than 1.4. The attrition rate stabilised at 40 operating hours, resulting in a long lifetime. [22]

Aturo Cabello et al. investigated a copper based oxygen carrier (Cu14γAl) produced with the wet impregnation technique. He evaluated the OC in a 500W CLC pilot plant and used methane as fuel. At conditions of 800°C and Φ=1.5-2, the methane combustion was completed. In addition to that it shows that the attrition was comparably good, as mentioned in previously. [23]

At the *Technische Universität Wien* a copper based OC, CuO/Al_2O_3, was previously investigated in the master thesis of *Zerobin* [24] in 2013 and was the Benchmark for this thesis. The difference to the OC is that it is produced in industrial scale whereas it was not in *Zerobin's thesis* 2013. *Zerobin* investigated that besides CH_4 there is also H_2 and CO in the FR exhaust gas stream. CO is very low at about 0.5vol%wet, whereas H_2 is up to 2vol%wet. Also *Luis de Diego et al.* [25] shows in pre-investigations of different copper based oxygen carrier (prototypes) that CO and H_2 appear at the reduction process. The result of the attrition rate, at *Zerobin*, was similar to other results mentioned before. The CuO content results in a steady-state condition after 30h. [24]

Reaction equations of the Cu15 OC: [14] [21] [24]

FR:

$$C_xH_y + xCuO_a \rightarrow xCO + \frac{y}{2} H_2 + xCuO_{a-1} \quad (12)$$

$$CO + CuO_a \leftrightarrow CO_2 + CuO_{a-1} \quad (13)$$

$$H_2 + CuO_a \leftrightarrow H_2O + CuO_{a-1} \quad (14)$$

AR:

$$Cu + \frac{1}{2}O_2 \rightarrow CuO \quad (15)$$

CLOU:

CLOU happens when the OC is interacting with the support material. Therefore, the active copper has to interact with the Al-support at specific temperatures. At higher temperatures the CuO reacts with the support material Al_2O_3 to form $Cu^{2+}Al_2O_4^{2-}$. The effect is that the redox reaction is changing: CuO - Cu_2O → CuO - Cu.

That results in a reduction of the equilibrium of the oxygen partial pressure. Nevertheless, the conversion abilities of the Cu-based OC are not affected. Therefore, CLOU reactions with the Cu15 OC are not expected. [22] [26]

2.2.4 Reactor System

The reactor system for a CLC process can be basically divided in fixed beds and fluidized beds. Normally the OC is the bed material itself. With fixed beds, the OC is drained alternatively by air, whereas the fluidized beds have a circulating OC. Most of the reactor designs have a minimum of two fluidized bed reactors. Those are connected with each other and the bed material (OC) is circulating between them. The connections between the reactors are the loop seals which are purged with steam or - CO_2. The benefit of the loop seals is that no gas exchange is possible between the reactors. [27]

Therefore, the CLC reactors are challenged to reach a couple of objectives, namely a good gas-solid contact between the air/fuel and the OC, low mechanical stress to prevent attrition on the OC, a good oxygen transport between the reactors (results from a good circulation of the OC between them) and sufficient bed material. But additionally, the OC characteristics must also be kept in mind when constructing reactor systems. These terms are the residence time of the OC in the FR and the AR, the inventory of the OC in those reactors and the circulation of the OC between the reactors. Furthermore, the temperature of the possible best performance of the OC is also important. All these points of the OC and the reactor system are necessary to achieve an optimised performance. [4] [16]

2.2.5 The Dual Fluidized Bed System

The dual circulating fluidized bed system (DCFB) is a technology where the reactors are connected to each other with loop seals. Those reactors are circulating fluidized beds and are called the AR and the FR. In the AR the OC gets oxidized with air, whereas in the FR the OC gets reduced, because of the fluidization with the gaseous fuel. The OC is transported from the AR to the FR via the upper loop seal (ULS) while the OC is transported from the FR to the AR via the lower loop seal (LLS). The internal loop seal (ILS) is only connected with the FR to recirculate the OC particles back to the bottom of the FR. [28] [16]

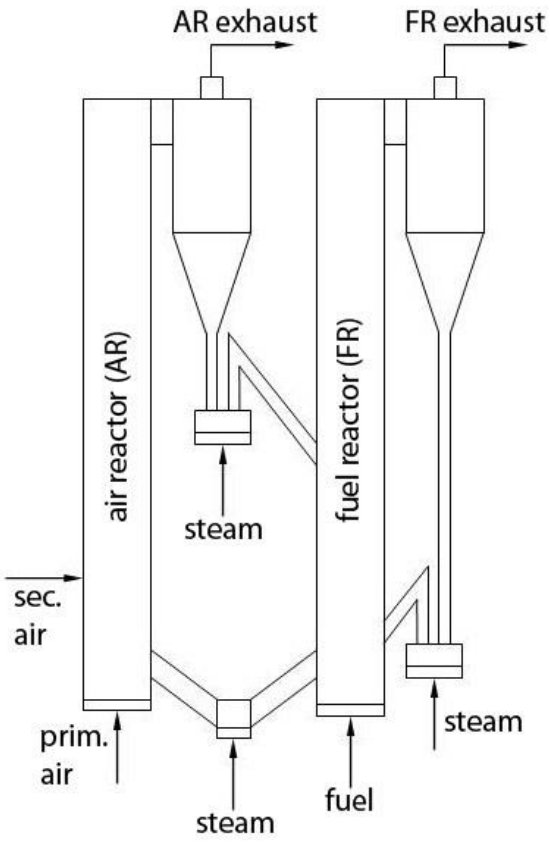

Figure 2. 6: Schema of the DCFB system for CLC (taken from [16])

One of the advantages of the DCFB is the creation of a good gas-solid contact by the two fluidized beds. Another benefit is that the global solid circulation is determined by the AR, to be precise from the AR fluidization rate, this means that the FR fluidization can be prepared separately from the AR. This leads to a better fuel conversion performance of the CLC process. [16]

3. EXPERIMENTAL

3.1 The 120kW Pilot Unit

The 120kW pilot unit, as mentioned in section 2.2.5, is based on the Dual Circulating Fluidized Bed system (DCFB). Figure 3. 1 shows the characteristics of the pilot plant. The different characteristics are the three loop seals, the two reactors and the cooling jackets. To prevent gas leakage between the reactors, the reactors are connected with loop seals. Those loop seals are fluidized with steam whereas the AR is fluidized with air and the FR is fluidized with gaseous fuels. The cooling jackets are an essential fitting at the AR to keep the reactor temperatures under control.

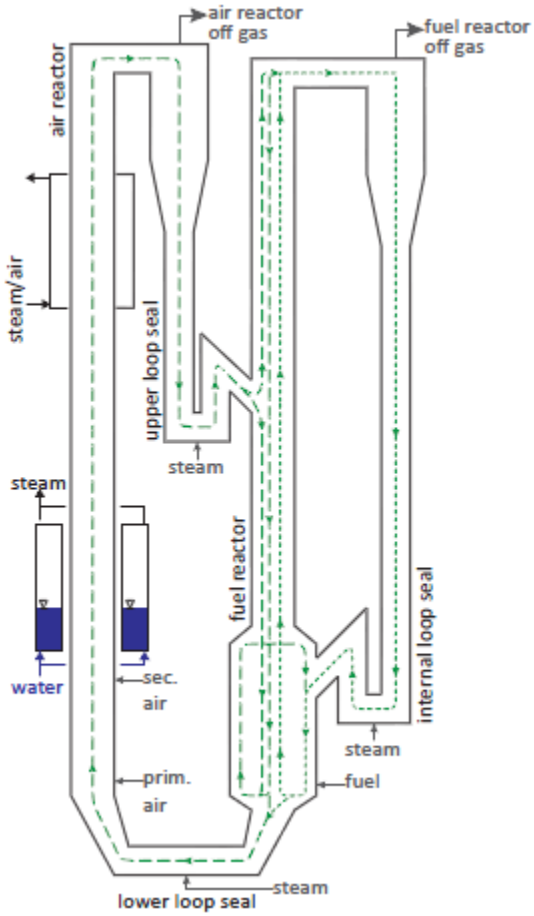

Figure 3. 1: Scheme of the 120kW pilot rig at the *Technischen Universität Wien*

In this thesis the FR is fluidized with gaseous fuels. During most operating points (OpPt) the FR is fluidized with natural gas. The natural gas is taken from the Viennese-Gas-Grid. The specifications are shown in Table 3. 1.

Table 3. 1: Specification of the natural gas from the Viennese-Gas-Grid

SPEZIES	VOL%
CH_4	96.73
C_2H_6	1.5
C_3H_8	0.43
CO_2	0.3
N_2	1.05
CO	0
H_2	0

For some investigations, the FR is not only fluidized with natural gas, it is also fluidized with higher hydrocarbons. Those are propane and pentane. Pentane, however, had to be evaporated through a vaporizer before it was sent into the FR. Therefore, a vaporizer with accompanying heating was installed. Propane was not liquid so it was not necessary to pass the vaporizer.

The exhaust gases of the two reactors are permanently analysed with online measurements. Carbon monoxide, carbon dioxide and oxygen are analysed in the exhaust gas of the AR. Carbon monoxide, carbon dioxide, methane, oxygen and hydrogen are analysed in the exhaust gas of the FR. To prevent water in the online measurements, the exhaust gases are cooled and the water is collected. After the FR the gases are collected and lead to the fire tube burner, where the gases are combusted. The last step is to filter the gas with a filter bag, to prevent particles leaving the chimney.

The upper part of Table 3.2 shows the dimensions of the pilot rig at *TUW.* The first tests at the pilot rig were done in 2008 by *Kolbitsch et al.* The lower part of Table 3.2 shows the design specifications of the pilot rig at the *TUW*. [29] [16]

Table 3. 2: Dimensions of the 120kW pilot rig and Design Specifications of the pilot rig at fuel power: 120kW and fuel ratio: 1.2

		UNIT	AR		FR
INNER DIAMETER AR		[m]	0.1297		-
INNER DIAMETER FR LOWER PART		[m]	-		0.1795
INNER DIAMETER FR UPPER PART		[m]	-		0.1023
HEIGHT		[m]	4.03		3.8
HEIGHT PRIMARY GAS INLET		[m]	0.025		0.02
HEIGHT SECONDARY GAS INLET		[m]	0.44		-
FUEL POWER		[kW]		120	
FUEL RATIO		-		1.2	
TEMPERATURE		[°C]	950		950
ARCHIMEDES NUMBER		-	6.9		6.78
SUPERFICIAL GAS VELOCITY AR		[m/s]	9.8		-
SUPERFICIAL GAS VELOCITY FR	**UP**	[m/s]	-		5.5
	LOW	[m/s]	-		1.8
INLET GAS FLOW		[Nm^3/h]	140		12
OUTLET GAS FLOW		[Nm^3/h]	114		36

3.2 Reduction Furnace

For analysing the solid samples of the particular operating points, a reduction furnace is used. Its scheme is shown in Figure 3. 2 and helps to analyse the oxidation state and the possibility of coking.

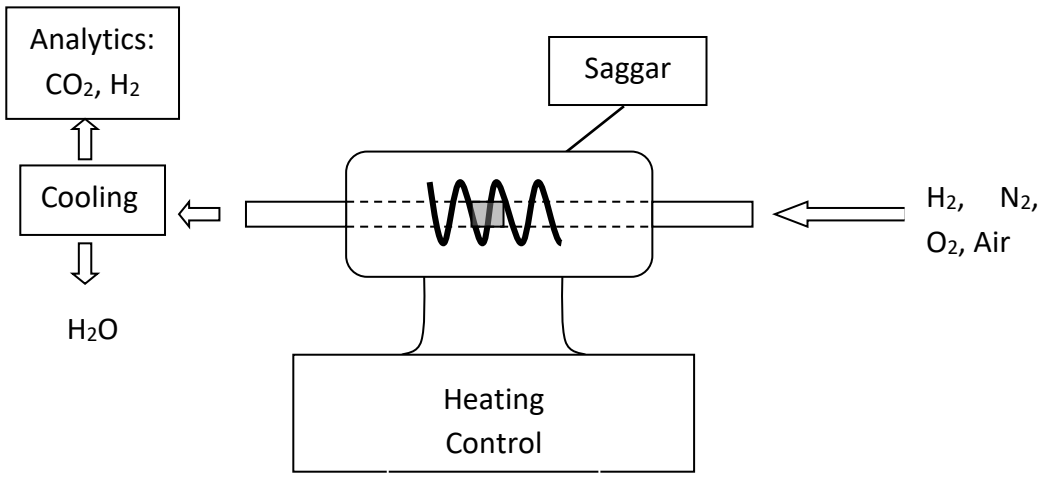

Figure 3. 2: Scheme of a reduction furnace

Setting of the furnace:

To get the right setting of the reduction furnace, the parameters have to be adjusted. The temperature must be set as well as a proper reduction time. In addition to that, the concentration of the hydrogen and nitrogen throughout the reduction must be set. After this, the samples are oxidized in a muffle furnace for at least five hours.

Oxidation procedure:

The solid sample of the OC is filled in a ceramic saggar, which is marked in grey in Figure 3. 2. The deadweight of the saggar and the filled one (with OC) is weighed and positioned in the middle of a ceramic tube. After that, nitrogen flows through the tube and the solid sample. When the analytics have not shown a sign of oxygen, the furnace is turned on. After 800°C is reached, air is switched on and is lead through the tube. When 900°C is reached, the temperature is held constant for a predetermined time. If coking happens in the pilot rig, CO_2 has to be seen at the analytics. When no CO_2 is detected anymore, the air is switched off and the furnace is cooled down in a N_2 atmosphere. When ambient temperature is reached, the ceramic saggar is weighed again to determine the weight gain.

Reduction procedure:

The sample is weighed, as in the above mentioned oxidation procedure, and also positioned in the ceramic tube. Nitrogen is also used as inert gas. At the beginning, nitrogen is lead through the tube, under ambient conditions, until no sign of oxygen appears in the analysis. After that hydrogen is switch on in addition to the nitrogen. The concentration has to be kept lower than the lower explosion limit, to avoid undesired ignition of hydrogen.

The furnace was heated up and kept constant at 900°C. As long as the sample is not fully reduced, H_2 is converted to H_2O (see equation 16). Therefore, the reduction runs until no H_2 is converted any more. That was able to see on the analytics, when the H_2 value has not changed any longer. The resulting water is deposited with the help of a condensation trap.

$$CuO + H_2 \rightarrow H_2O + Cu \quad (16)$$

After the input concentration is reached, hydrogen is turned off and the sample is cooled down to ambient temperature under inert conditions. When ambient temperature is reached, the saggar with the OC is reweighed to get the reduction mass and the weight loss.

3.3 Analytics

In every single experiment different analytical methods were used. Analytical methods for gases as well as solid samples are applied during and after the experiments. This chapter explains in detail the methods used.

3.3.1 Solid Analytics

A solid sample is needed to determine the different oxidation states of the operating points. Solid samples from ULS and LLS are taken for every operating point.

Solid sampling:

To further analyse the oxidation state of the OC of an operating point the solid sampling procedure has to be done. Figure 3. 3 shows the general procedure. This procedure makes it possible to get a sample of the oxygen carrier during operation. After taking the samples, they are cooled down in an inert atmosphere (Argon). Normally two solid samples of each operating point are taken, the first one of the ULS and the second one of the LLS of the power unit. The whole procedure is described by *K. Mayer* [20].

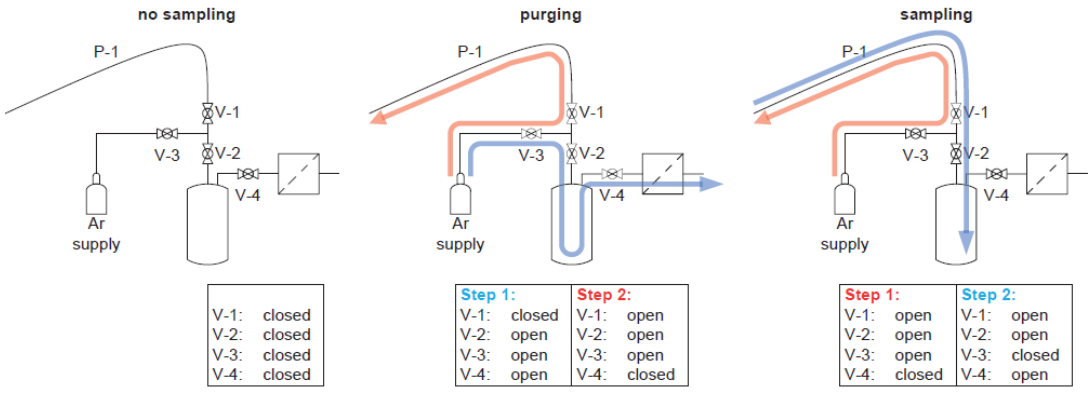

Figure 3. 3: Solid sample procedure (taken from [20])

After the solid samples were taken, they were weighed and dried. Following the drying process, the solid samples are treated in a muffle furnace at 900°C to get fully oxidized and afterwards they are weighed again. In addition to this treatment, the solid samples are used for X-ray fluorescents analysis (XRF) or Thermo gravimetric analysis (TGA) or

for the reduction furnace - mentioned in section 3.2. Thus, more information about the OC after the CLC process can be obtained.

The TGA helps to determine the oxygen transport capacity (R_0) and the active metal content of the OC (for example Cu), whereas the XRF analysis is a method to determine the different elemental components in a sample. In this thesis the XRF analysis is used to determine the Cu components in the OC. The OC used in this study, called Cu15, is mainly composed of CuO and Al_2O_3. The following table shows the result of an XRF analysis for an operating point.

The get more information of the physical characteristics of the used oxygen carrier the bulk density and the mean particle size was analysed. The results are 841 kg/m^3 and 153µm.

Table 3. 3: Example of an XRF result for an operating point

	SAMPLE
ELEMENTAL COMPONANTS	**[%]**
$\mathbf{ZrO_2}$	0.01%
$\mathbf{CuO}$	16.03%
$\mathbf{NiO}$	0.03%
$\mathbf{Fe_2O_3}$	0.09%
$\mathbf{MnO}$	0.37%
$\mathbf{Cr_2O_3}$	0.03%
$\mathbf{TiO_2}$	0.18%
$\mathbf{CaO}$	0.19%
$\mathbf{K_2O}$	0.01%
$\mathbf{Cl}$	0.07%
$\mathbf{SO_3}$	0.04%
$\mathbf{P_2O_5}$	0.05%
$\mathbf{SiO_2}$	0.75%
$\mathbf{Al_2O_3}$	82.15%

3.3.2 Gas Analytics

Online analytics:

Online measurements were recorded through the whole campaign. Generally, the composition of three gas streams can be measured: (1) the AR exhaust gas stream, (2) the FR exhaust gas stream and (3) the Fire tube burner (FTB) gas stream. For protecting the measurements from the condensing water, a condenser is placed before the inlet

of the analytics. After that, the dry gas can be lead to the analytics and the different components of the gases are sent to the computer system. [20]

Gas Chromatography:

In addition to the online analytics a Gas Chromatography (GC) is used. This GC takes a sample form the FR exhaust gas every 15min. Therefore, every single operating point has at least one GC sample. This analytic is compared to the online analytics and is also used for the evaluation of the operating points. The components which are measured with GC are:

Table 3. 4: GC components

CO_2	CO	CH_4	C_2H_4
C_2H_6	N_2	O_2/Ar	C_3H_8

3.4 Data Evaluation

The simulation software used in this thesis is called *Integrated Process Simulation Environment (IPSEpro)* and was developed by Simtech.

3.4.1 Integrated Process Simulation Environment

IPSEpro is a simulation tool which the user can operate very easily on a graphic flowsheet modelling interface, using the Advanced Energy Technology library (AET-lib), which includes all different equations for the process.

The flow sheet of the 120kW pilot plant can be seen in Figure 3. 4 and includes different units, which are taken from the model library. Each of these units contains different equations describing the process. This process can be validated by energy and mass balances; therefore, data has to be measured, and must be loaded into the system. This data is taken from measurements of the steady state operating points and is therefore a static model.

All the data of the measurements and the data of the balances lead to an over-determined system. To solve this system, the Langrage multiplier method, which means that the smallest square of the difference of the measured data and the equalized solution divided by the absolute tolerance, is used. This tolerance tol_{xi} value is different for each measured value and can be chosen individually.

In addition to this the process values which are unknown can be calculated with the simulation model. [24]

$$\sum_i \left(\frac{x_i - \bar{x}_i}{tol_{x_i}}\right)^2 \rightarrow \min \tag{17}$$

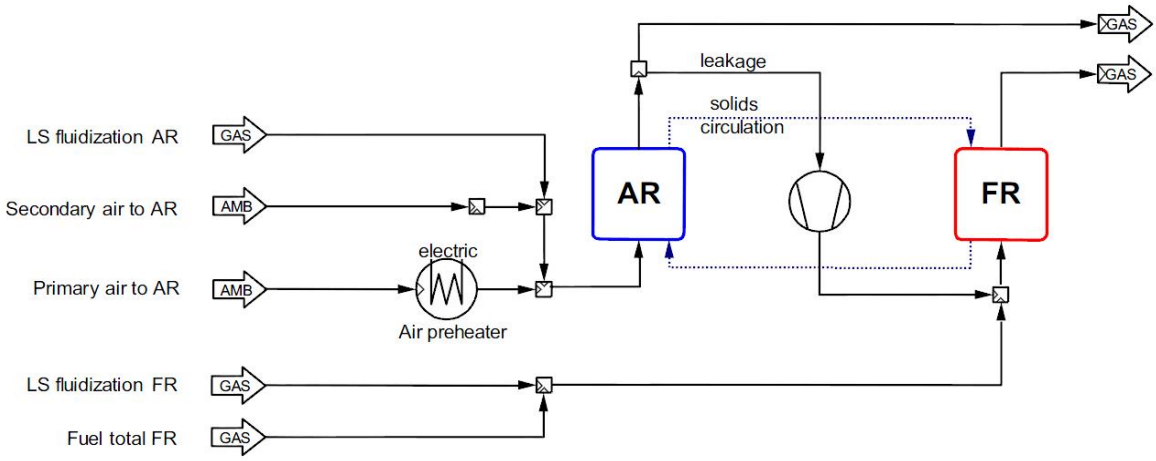

Figure 3. 4: Simulation of the 120kW pilot rig in IPSEpro

Figure 3. 4 shows the IPSEpro flow sheet. This model was used for every operating point. The whole plant is shown including the gas leakage to the FR. Additionally, the solid circulation is shown between the AR and the FR.

In sections 4.4.2 and 4.4.3 a sensitivity analysis of possible inconsistencies of different parameters is discussed and explained, because of the problem of measuring the X_S. This analysis helps to verify the problems of which value is the most affected by changing specific values.

With the help of a statistic error in the evaluation process, a statement of the conditions of the process can be done. It shows how good the evaluation works with the implemented values to the simulation program. Every change of a value will change the statistic error. Therefore, a change of a designated parameter, like in the sensitivity analyses, will have an effect on the statistic error.

4. RESULTS AND DISCUSSION

The OC, that was used, was tested in a 120kW pilot rig which is described in section 3.1. In addition to this, a sensitivity analysis of specific parameters was made. To compare the results, the used parameters which are shown in the next section 4.1 are essential.

At the *Technische Universität Wien, Penthor et al.* previously investigated a CuO/Al_2O_3 OC in 2013. But not only the TUW has investigated a copper-based OC, also the *Consejo Superior de Investigaciones Cientificas (CSIC)* have also previously developed and analysed it. [26]

To compare that with previous work, the total inventory range is less (approx. 10kg) than in this study. Also, the fuel power is studied more in detail and over a wider range. In this thesis the fuel power is analysed from 50.56kW to 93.09kW, whereas in previous work, the fuel power is analysed from 60kW to 70kW. A bigger fuel power range leads to a bigger range for the specific inventory. [24]

The higher hydrocarbons were analysed to determine and compare the effects of increases in the different mixtures on efficiency. In general, a good conversion is very important because of the contaminations of other species, besides steam or CO_2 in the FR exhaust gas. Those contaminations will lead to more complicated separation of the exhaust gas.

4.1 Parameters Used

To analyse the operating points, different parameters are used and discussed. The following ones are important for the CLC process. In this thesis all of them are used to compare the performance of each operating point.

The conversion performance of each species is described with the following equation.

Conversion performance X_i:

$$X_i = 1 - \frac{\dot{n}_{FR,exh} * y_{i,FR,exh}}{\dot{n}_{FR,feed} * y_{i,FR,feed}} \quad (18)$$

i = for example CH_4.

Another parameter for the performance is the CO_2 yield. In the case of a full conversion, the yield will be 100%. But the yield drops because of incomplete conversion, which means that there are more carbon components in addition to CO_2 in the exhaust gas.

CO_2 Yield:

$$Y_{CO2} = \frac{\dot{n}_{CO2,FR,exh}}{\dot{n}_{C,FR,exh}} \tag{19}$$

The combustion efficiency (η) will be also 100% if all heating value is converted to carbon dioxide. The LHV is the lower heating value of the FR exhaust gas or feed.

Combustion efficiency η_{comb}:

$$\eta = 1 - \frac{\dot{n}_{FR,exh} * LHV_{FR,exh}}{\dot{n}_{FR,feed} * LHV_{FR,feed}} \tag{20}$$

λ is the air to fuel ratio. It describes the ratio of the available oxygen to the necessary oxygen for complete combustion.

Air to fuel ratio λ:

$$\lambda = \frac{\dot{m}_{O2,AR,feed}}{\dot{m}_{O2,FR,stoichometric}} \tag{21}$$

The global solid circulation rate is the mass flow of the solids circulating between AR and FR related to the AR cross section.

Global solid circulation rate G_s:

$$G_s = \frac{\dot{m}_{OC}}{A_{AR}} \tag{22}$$

Oxygen transport capacity describes the amount of O_2 that can be transported by the OC related to its mass.

Oxygen transport capacity R_0:

$$R_0 = \frac{m_{OX} - m_{RED}}{m_{OX}} \tag{23}$$

The particle oxidation state is the average oxidation state of the solid sample. It is defined as the mass difference of the actual sample and the most reduced form divided by the fully oxidized and reduced form of the solid sample. Therefore X_s=0% means that the sample is fully reduced, whereas X_s=100% means the sample is fully oxidized.

Particle oxidation state X_s:

$$X_s = \frac{m - m_{RED}}{m_{OX} - m_{RED}} \tag{24}$$

The difference of the particle oxidation state of the particular reactors is called ΔX_s. It describes the different oxidation states in the FR and the AR. Naturally the oxidation state in the AR is higher than in the FR. The oxidation state is an important input data of the simulation program.

ΔX_s:

$$\Delta X_s = X_{s,AR} - X_{s,FR} \tag{25}$$

The OC to fuel ratio is an important parameter to show the oxygen supply to the FR. Parameter b is the stoichiometric CuO quantity for complete fuel conversion. [24]

OC to fuel ratio Φ:

$$\phi = \frac{\dot{n}_{CuO}}{b * \dot{n}_{fuel}} \tag{26}$$

$$\mathrm{b} = \frac{4x_{CH_4} + 10x_{C_3H_8} + 16x_{C_5H_{12}}}{x_{CH_4} + x_{C_3H_8} + x_{C_5H_{12}}} \tag{27}$$

In section 4.4 a sensitivity analysis is done. Therefore, a parameter is described to compare the results in detail. C_{CuO} is the CuO content in the OC of the particular analysed samples. Whereas $C_{CuO,0}$ is the CuO content of the operating point. ΔQ_i describes the difference of the analysed parameters. These are the OC to fuel ratio, the global solid circulation rate and the statistic error of the simulation program. Q_0 is the operating point value of these parameters, whereas Q_i is the calculated value of C_{CuO}. The sensitivity parameter is a good corresponding parameter to use to get a better look at the difference and strong deviation of the changed operating points.

Sensitivity parameter ξ:

$$\xi = \frac{\frac{\Delta Q_i}{Q_o}}{\frac{\Delta C_{CuO}}{C_{CuO,0}}} \tag{28}$$

Inventories:

The total bed inventory describes the whole inventory which is present in the reactor system, the reactors and the loop seals. The difference between the total bed inventories in this thesis is 4kg.

In contrast to the total inventory, the active inventory is the material which is present in each of the reactors. That means that only the inventory which is in a reaction is the active inventory. It can be calculated with the pressure drop in each reactor. And the sum of the two inventories is the total active inventory.

$$\mathrm{m}_{\mathrm{act\_Inv}} = \frac{\Delta p * A_r}{g} \tag{29}$$

That range is between 8.41kg and 16.66kg.

The specific inventory also has to be mentioned. This inventory depends on the active inventory of the AR or the FR based on the fuel power. And the total specific inventory is therefore the sum of the two. That range is about 120.07kg/MW to 314.19kg/MW, with the fuel power range of the operating points of 50.56kW to 93.09kW.

4.2 Cu15 Performance

The range of the used parameters is shown in Table 4. 1. To compare the different operating points, only one descriptive parameter is changed, affecting as little other parameters as possible. It is aimed to hold other parameters at the standard operating conditions. These are shown in Table 4. 2.

Table 4. 1: Inventory ranges of the OC (Cu15) of the analysed operating parameters

	UNIT	CU15
BED MATERIAL TOTAL INVENTORY	[kg]	40-44
TOTAL ACTIVE INVENTOY	[kg]	8.41-16.66
AR ACTIVE INVENTORY	[kg]	1.69-5.26
FR ACTIVE INVENTORY	[kg]	6.73-11.45
TOTAL SPECIFIC INVENTORY	[kg/MW]	120.07-314.19
AR SPECIFIC INVENTORY	[kg/MW]	24.08-98.87
FR SPECIFIC INVENTORY	[kg/MW]	96.00-215.32
FUEL POWER	[kW]	50.56-93.09

Table 4. 2: Standard operating conditions for the Cu15 oxygen carrier

	UNIT	STANDARD CONDITIONS
BED MATERIAL TOTAL INVENTORY	[kg]	40
AIR TO FUEL RATIO	[-]	1.5
TEMPERATURE	[°C]	800
FUEL POWER	[kW]	70
FUEL		Natural gas

4.2.1 Effect of Fuel Power and solid inventory

During the whole campaign the fuel power values were changed between 50kW and 90kW and the FR specific inventory between 96kg/MW and 215.32kg/MW.

It is important to know that the fuel fluidised the FR. The effect of this is that the fluidisation regime is changing with the changing fuel power. This has effects on the methane conversion, which can be seen in Figure 4. 1. At the lower fuel power values, the methane conversion is the highest.

It must also be mentioned that the CuO content of the particles is changing over time. Therefore, fresh particles will have a better conversion performance than used ones. At 60kW the particles are fresh material. At 50kW the particles are at the beginning of one experimental campaign. The other four points are used material and therefore the

CuO content of the particles will be lower because the attrition through the whole experimental campaign influences the specific FR inventory. A similar behaviour was determined by *Penthor et al*. This effect can be seen in Figure 4. 1. [24] [26]

In Figure 4. 2 can be seen that a higher inventory leads to a higher specific inventory. From this point it can be concluded that more inventory in the FR leads to a higher contact between the gas and solid materials. The consequence is that more inventory in the FR leads to a higher methane conversion and a higher carbon dioxide yield.

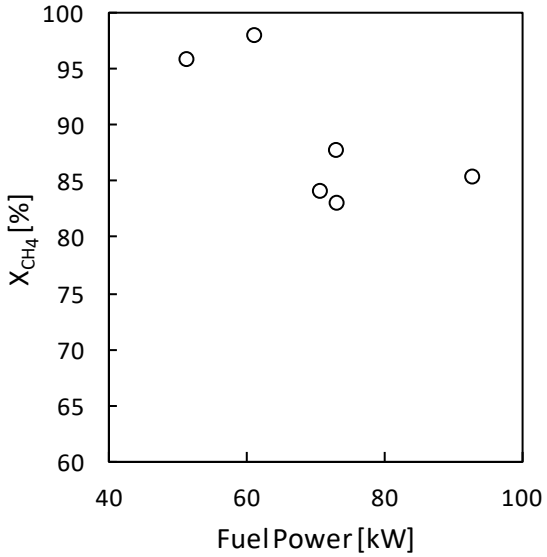

Figure 4. 1: Changes of the methane conversion at different fuel power values

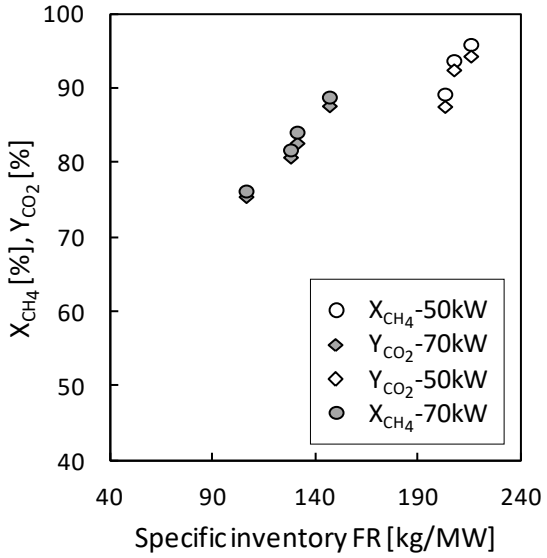

Figure 4. 2: Different effect on the methane conversion and carbon dioxide yield at different specific inventories

4.2.2 Effect of Temperature

Another parameter which influences the performance of the Cu15 oxygen carrier is the temperature. The standard operating temperature in the FR is 800°C, but to see the influence of temperature on the CLC process the temperature must be varied for some OP between 800°C and 900°C which is shown in Figure 4. 3.

The measurements of the temperature show a linear effect on the fuel conversion. The black points represent online measurement data, whereas the white points represent validated operating points. Both data confirm that linear behaviour, which can be seen in Figure 4. 3. The OpPt are measured at 70kW and between 112.73kg/MW and 133.61kg/MW in the FR. In addition to these parameters the air to fuel ratio is between 1.42 and 1.48.

At 900°C, nearly full methane conversion was achieved. It can be concluded that a higher temperature leads to a better performance of the CU15 OC and therefore to a higher fuel conversion.

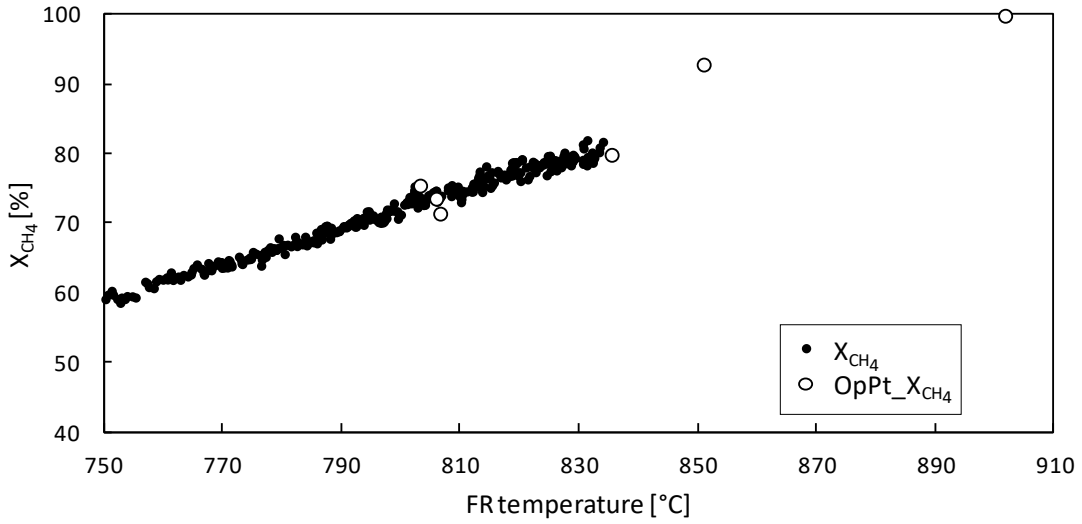

Figure 4. 3: Behaviour of the methane conversion at different temperatures. X_{CH4} are the online measurement values and OpPt_X_{CH4} are the operating points values

To get a closer look at the influence of the temperature on the conversion performance, the FR exhaust gas can be analysed. In Figure 4. 4 it can be seen that the components of the FR exhaust gas (CH_4, CO, H_2) show incomplete conversion except for the last point at 900°C (FR specific inventory: 127.59kg/MW; λ=1.42). It also shows that higher temperatures have a positive influence on the conversion.

The especially low CO value stands out. One possible explanation is that CO reacts with steam to form CO_2 and H_2. The higher H_2 value occurs because of the water-gas shift reaction and also because of the steam reforming reaction.

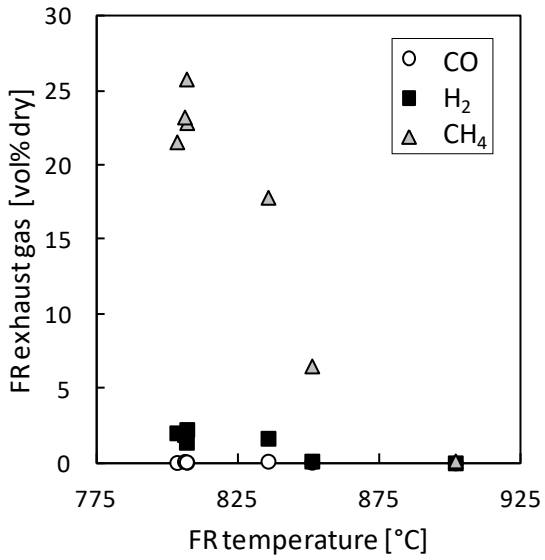

Figure 4. 4: Components of the FR exhaust gas at different temperatures (λ=1.4-1.49; T_{FR}=803.21-901.72; 71.16-74.10kW)

4.2.3 Influence of the Air Reactor (AR)

Another very important fact to know is whether the AR limits performance. That means: are the particles able to get fully oxidized in the AR or not? That implies testing to see if the oxidation state of the particles is limited to a stagnant value. Another research question is also how the methane conversion behaves when the air to fuel ratio is varied.

Influence of the air to fuel ratio:

The air to fuel ratio (λ) describes the oxygen concentration and the fluidization in the AR. With the primary and the secondary air supply, the volume flow of the air, in the AR, can be set.

The operating conditions in Figure 4. 5 and Figure 4. 6 are the same. The temperature is between 799°C and 806°C and the total active inventory is between 11.21kg and 13.71kg**.** Figure 4. 5 (a) shows the mean residence time of the solid in the AR with different λ values. It can be seen that a significant trend is not obvious. In addition to this, the methane conversion (Figure 4. 5 (b)) also shows no significant trend.

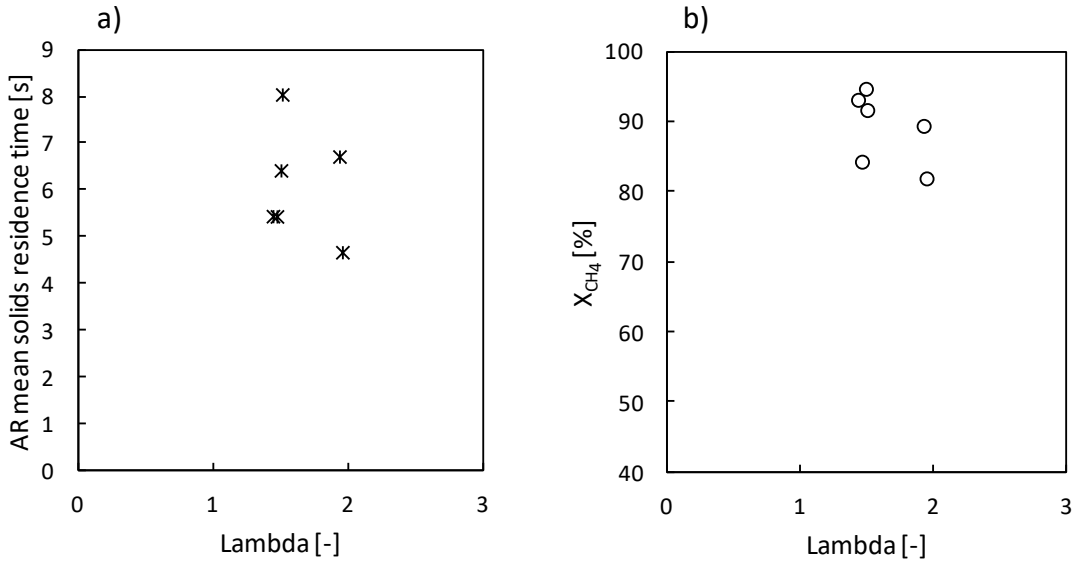

Figure 4. 5: (a) Effect on the AR mean solids residence time with different Air to fuel ratios; (b) Influence on the methane conversion by using different air to fuel ratios

The AR solid residence time has an effect on the oxidation state of the particles. In Figure 4. 6 (a) can be seen that the oxidation state is nearly stagnant at 70%. That will lead to the assumption that the AR is limited. However, determination of the oxidation state of particles showed a systematic error (see Section 4.4) and absolute values for X_s are not fully liable.

In Figure 4. 6 (b) a tendency can be seen of the increasing methane conversion with a longer solids residence time in the AR.

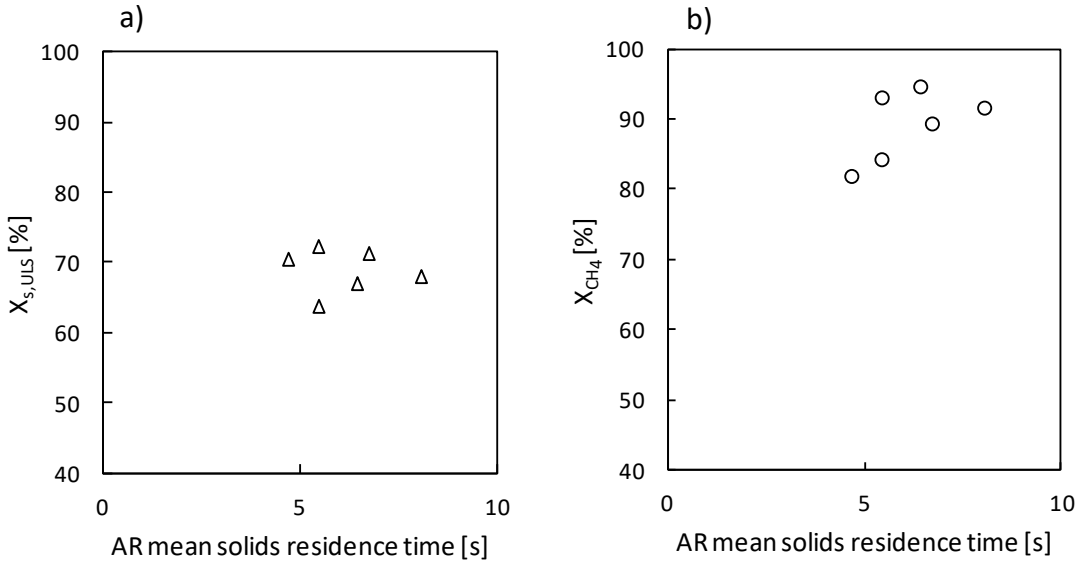

Figure 4. 6: (a) Influence of the AR solid residence time on the CuO oxidation state in the upper loop seal; (b) Methane conversion on the AR solid residence time

Air staging and particle oxidation state:

For air staging, the secondary air supply is used in conjunction with the primary air. That means that the circulation can be varied by increasing the secondary air supply, while leaving the total amount of air constant. The AR prim air ratio is the percentage of the primary air in the system. Therefore, it is the primary air divided by the sum of primary air and secondary air.

It can be seen that a higher active inventory and a higher secondary air supply causes a higher methane conversion. Therefore, a lower inventory and a lower secondary air supply causes a lower methane conversion because there is less oxygen transported to the FR (Figure 4. 7).

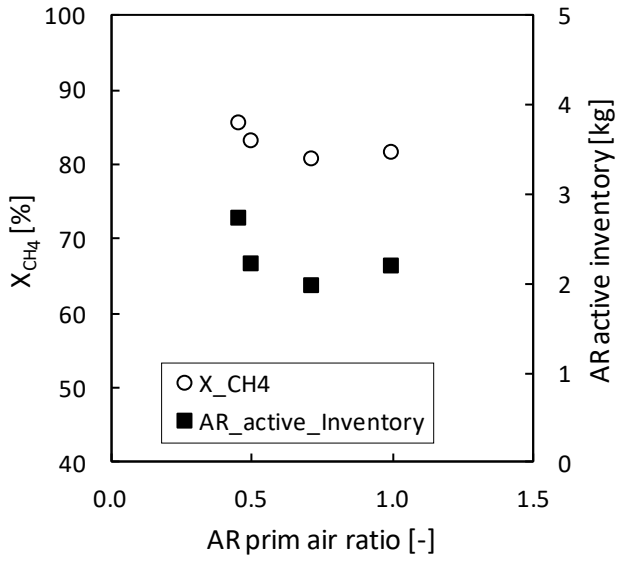

Figure 4. 7: Influence of air staging in the AR

In Figure 4. 8 it can be seen that the $X_{s,ULS}$ has no significant behaviour, rather stagnant, on higher global circulation rates. Therefore, a comparison of the oxidation states to previous work is difficult. The observations of the measurement of the particle oxidation state are problematic due to the standard measuring procedure itself. Based on those observations a sensitivity analysis was done and is described and explained in section 4.4. In that analysis it can be seen how different the sample weight and oxidation states affect other parameters.

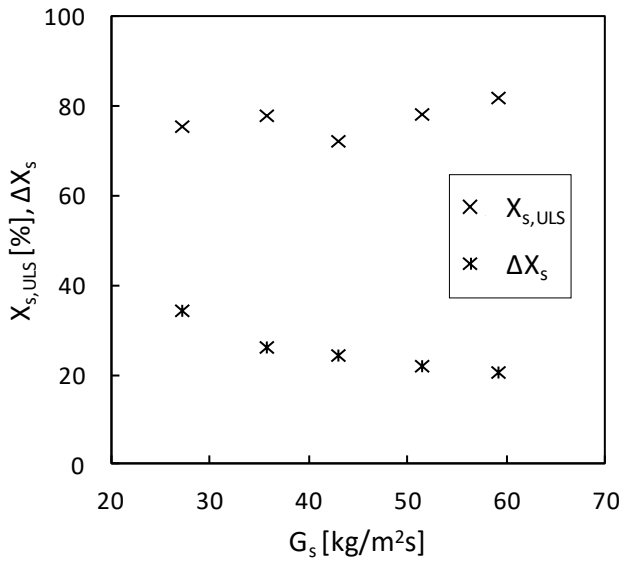

Figure 4. 8: Influence of the global circulation rate on the methane conversion

4.2.4 Influence on the Solid Circulation

The solid circulation depends on the total solids inventory and on the fluidization rate of the AR. So, the main parameter is the primary air supply to change the circulation.

The operating conditions in Figure 4. 9 are at λ=1.4-1.5, the temperature is 800-807°C and the fuel power is 70-76kW. Here it can be seen that a lower circulation rate has a negative effect on the methane conversion, with an increasing global solid circulation rate the methane conversion increases too. The explanation is that a low circulation rate leads to a low oxygen amount in the FR.

Normally the oxygen carrier to fuel ratio is taken to quantify the process performance. The problems which occur with the determination of the particle oxidation state – which is described in more detail in the sensitivity analysis in the next chapter – have effects on the oxygen carrier to fuel ratio. The problems with the absolute values of the oxidation state leads to an unreliable OC to fuel ratio.

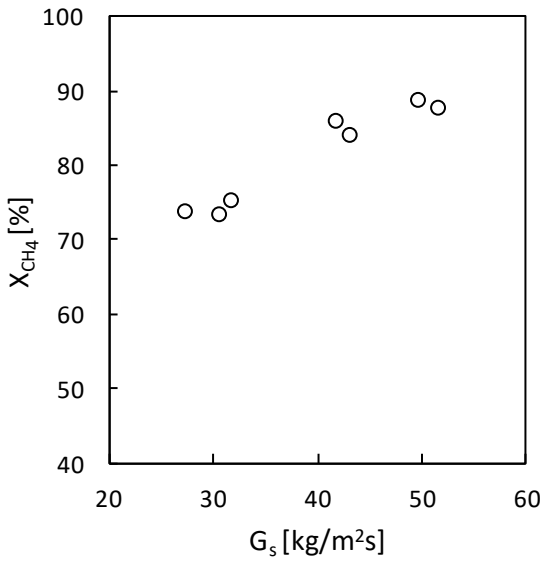

Figure 4. 9: Effect on the methane conversion with different global solid circulation rates

4.2.5 Attrition of the OC

The OC is under permanent stress during the CLC process. This can be mechanical stress (particles hit each other; particles bounce on the power rig walls), thermal stress (high temperatures) and chemical stress like reduction or oxidation reactions. All forms of stress results in weakening of the particles. Besides attrition, elutriation also occurs in the process. Elutriation is especially present at the beginning of each campaign and happens because the cyclone of the pilot plant is not designed for this material. Therefore, fine particles leave the power rig.

Figure 4. 10 shows the material loss over time (CLC OpPt time; start up not included) for every single operating point during the experiments 2 and 3. At the beginning it can be seen that the elutriation of the fine particle dominates. That means that small particles leave the pilot plant and they are not recirculated. After the elutriation at the beginning the material loss drops significantly to a small amount - between 0.1kg/h and 0.4kg/h (without the solid sampling). The peaks at about 180min can be attributed to higher temperatures and higher fuel power than before.

But in addition to attrition and elutriation, solid sampling is also a driver for material loss during the campaigns. Solid samples are taken at every single operating point from the ULS and the LLS. The loss of the solid sampling is about 0.38kg/h during the whole experiment 2 (weighted after the experiment). The average material loss of the

experiment 2 is 0.75kg/h. Therefore, the attrition and the elutriation are the difference of those values. These calculations were carried out for every operating point.

After the elutriation at the beginning the material loss drops significantly to lower values than 0.56kg/h (including the solid sampling).

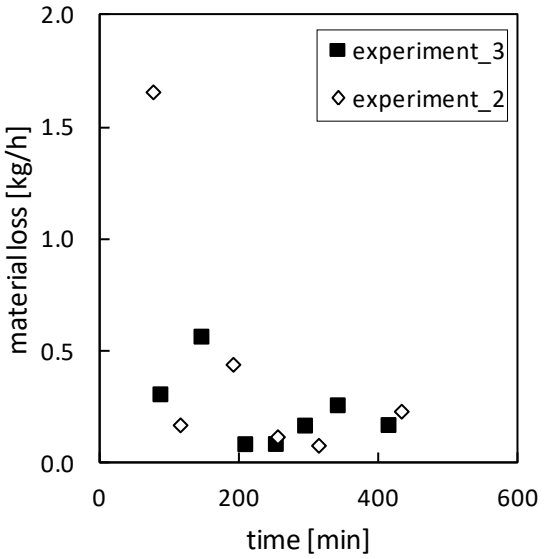

Figure 4. 10: Effect on the material loss (including the solid sampling) over time of the experiments 2 and 3

Figure 4. 11 shows the material loss (also including the solid sampling) over the air reactor exit superficial velocity. It explains that the material loss decreases with a higher AR exit superficial velocity. This could be explained with the conclusion that the cyclone is not designed for such small particles with low density. That means that a higher entrance velocity is necessary to be able to achieve the same critical size of the particle as in the design case. Furthermore, a higher solid load capacity leads to a better separation in the cyclone.

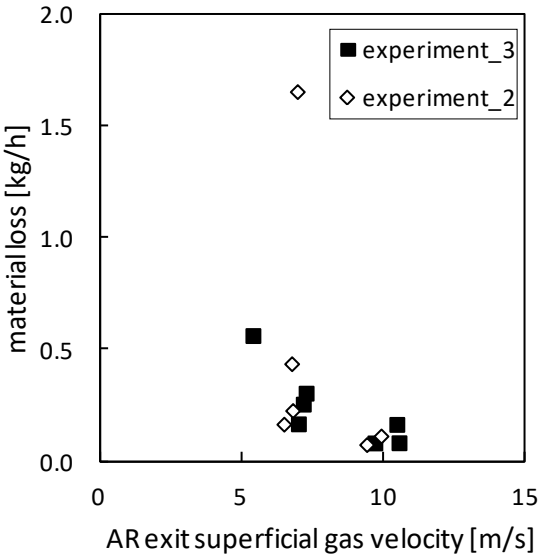

Figure 4. 11: Effect on the material loss over the AR exit gas velocity of experiment 2 and 3

4.2.6 Pressure Profile of the reactor

Figure 4. 12 shows the pressure profile for one operating point during the experiment. The pressure profile shows the AR and FR down comer and the three different loop seals and the reactors itself. It can be seen that the pressure drop in the AR is nearly constant through the height of the pilot rig. That means that the particles are distributed very well in the reactor – typically a fast-fluidized bed.

In the FR the pressure drop is much bigger at the bottom of the reactor which leads to a stronger dense bed than in the AR. This also explains the pressure difference in the lower and upper loop seals, which indicates that they are full of OC material. It is very important that no gas transfer between these two reactors happens. The ULS tends to choke sometimes, so it has to be observed carefully during the experiments. This can lead to a stop of circulation.

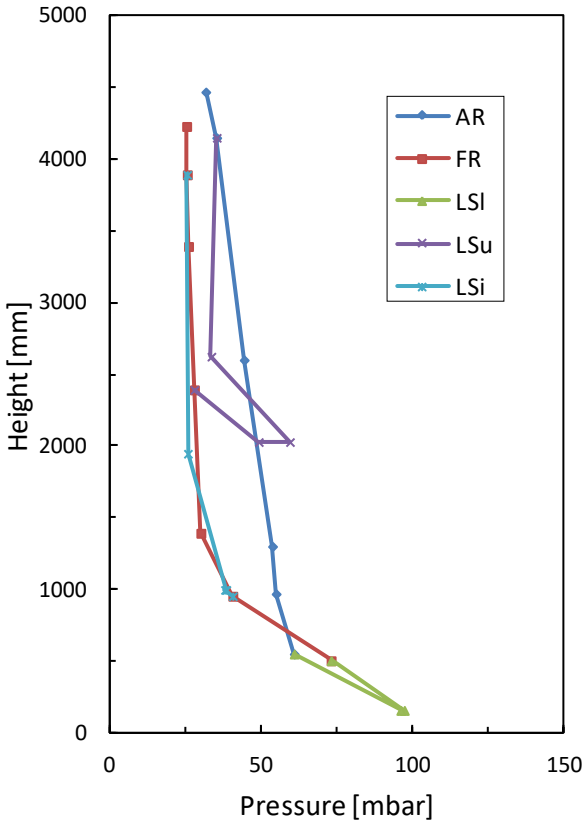

Figure 4. 12: Pressure profile of an operating point during an experiment

4.3 Conversion of Higher Hydrocarbons in the CLC Process

Higher hydrocarbons are also analysed in this thesis, because refineries use more fuels than only natural gas or methane. Therefore, propane and pentane are analysed in different mixtures among themselves and with natural gas. Those mixtures give some indication of the efficiency and the conversion of each species.

Five mixtures of natural gas, propane and pentane have been used and analysed. Standard conditions are λ=1.5, the temperature is T_{FR}=805°C and the fuel power is 70kW. It can be seen that the first mixture has a different fuel power (57kW, λ=1.8), because of problems at the setting, which is fixed after the first run.

Figure 4. 13 shows the different mixtures of the hydrocarbons in the feed gas and the composition of the exhaust gas of the FR. It has to be mentioned that the species are normalized on 100% carbon. Argon, nitrogen and hydrogen are also detected in the FR exhaust gas but were not considered. These gases constitute up to 7.5% of the exhaust

gas. It can be also seen that amount of C_2H_4, C_2H_6 and CO in the exhaust gas is very low.

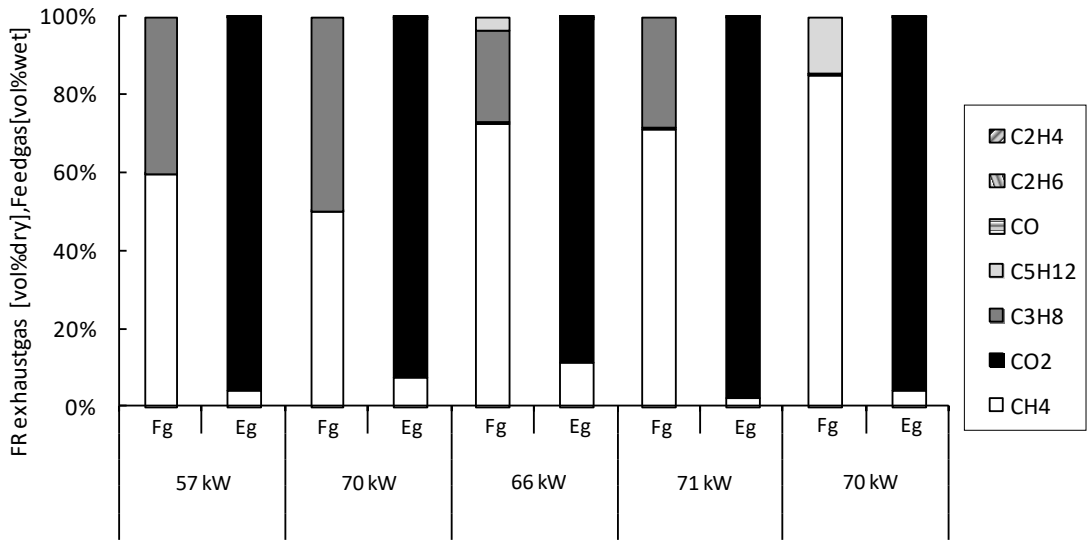

Figure 4. 13: FR exhausts gas and feed gas compositions at each operating point; T_{FR}=804-806°C

In each operating point a small amount of unburnt fuel, especially methane (up to 11.6%), in the FR exhaust gas is clearly evident. It can be also seen that nearly no higher hydrocarbon is detected in the FR exhaust gas stream.

To compare the results with previous works like *Zerobin's* [24], Figure 4. 14 is able to match them. First, it has to be mentioned that the operating conditions are 800°C in this work and 850°C in *Zerobin's* [24]. It can be seen that CO_2 yield and the efficiency is higher than what occurs in the different mixtures, compared to those of *Zerobin*. The CO_2 yield in *Zerobin's* thesis is constant at about 80%, whereas it can be seen in Figure 4. 14 that the CO_2 yield is higher at about 90%. The same behaviour can be seen in the efficiency. In both cases, the lowest carbon dioxide yield is at that OpPt where all three species are mixed in the feed gas.

Another point, which has to be mentioned, is that nearly no carbon monoxide was detected. The maximum of CO was established at the second OpPt and is about 0.4%.

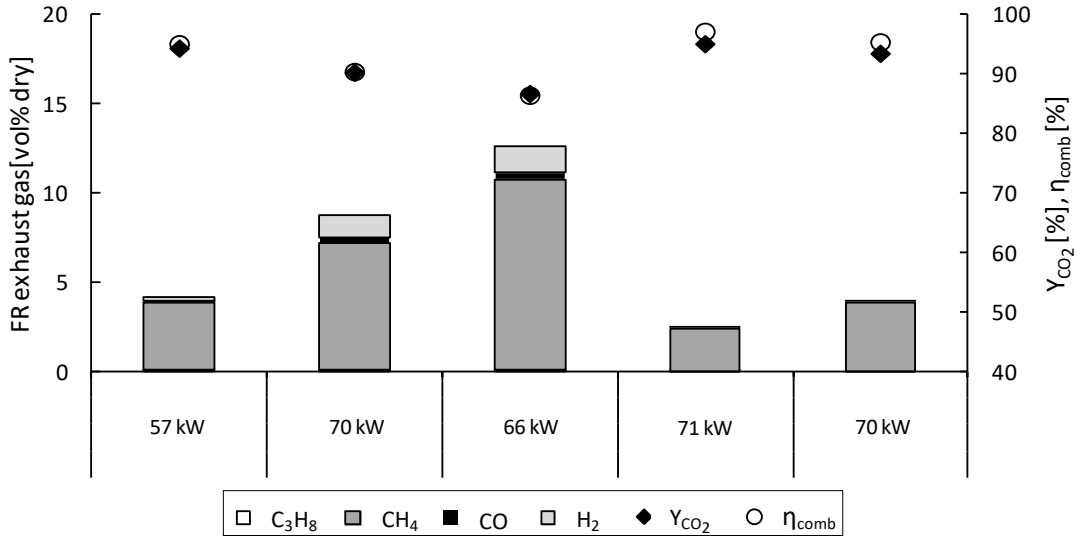

Figure 4. 14: Operating points of different hydrocarbon mixtures and their carbon dioxide yield and efficiency

To compare the higher hydrocarbon (HHC) operating points with those using only natural gas, Figure 4. 15 give information about the conversion efficiency. It can be seen that the specific solid inventory is a critical parameter for the HHCs as well. The trends of the efficiency of both analysed operating points (higher hydrocarbons and natural gas) are the same. Therefore, a higher FR specific inventory leads to a higher efficiency.

At lower specific solid inventories, the difference of the conversion efficiency of n.g. OpPt to HHC OpPt is bigger than at higher specific solid inventories in the FR. So, the efficiency of higher hydrocarbons with lower FR specific inventory is greater than those with natural gas. This is because of the much greater CO_2 yield at the HHC operating points.

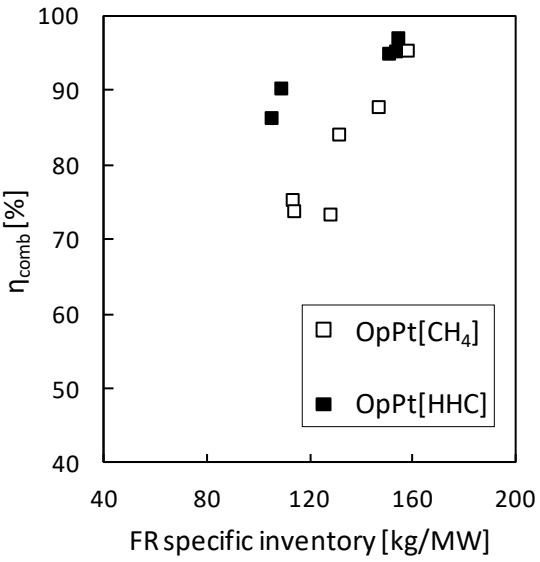

Figure 4. 15: Effect of higher hydrocarbons on the CLC process compared with methane operating points; (operating parameters in this diagram are λ=1.4, fuel power P=70kW and temperature T=800-807°C)

4.4 Validation of methods for determination of oxidation state and solids circulation

Because of uncertainties in the determination of the oxidation state of the solid samples a sensitivity analysis was done. These uncertainties appear during the measurements of the X_s of the samples. Therefore, a study of different parameters was performed because the absolute value of the X_s fluctuates. This will lead to a better understanding and possible improvements of the solid analysis.

The validation was performed to verify if the oxidation state has an impact on Φ or G_s and therefore on the general performance. So, the analysis helps to verify which parameter is “credible” and which is not.

Two parameters are analysed according to their influence on the oxidation state:

- The CuO content of the OC particles
- Mass of the solid sample during the weighing

It must be noted that the values of the CuO content were obtained by different analyses. Those analysed results are inconsistent. These used methods are:

- XRF analysis at the *TUW*
- TGA analysis by *CSIC*
- Reduction furnace at the *TUW*

One potential source for an error is the oxidation of the solid samples at ambient conditions. In order to evaluate this effect, the solid samples, which were taken during the experiments, were filled in a ceramic ship. These samples were exposed to ambient conditions and were weighted for several times over a certain period. This procedure was done for a sample of the ULS and the LLS.

Figure 4. 16 shows the influence of the weight of the solid sample under ambient conditions over time. Especially in the first 250 minutes a significant increase is noticeable. After that the sample mass stagnates. Increases of 2.21% of the ULS and 2.23% of the LLS are shown. The mass of the sample increases generally because the copper reacts with air (oxidation) under ambient conditions.

Another aspect is that the mass of the LLS increases faster than the mass of the ULS solid sample. This is an indicator that oxidation happens, because the lower loop seal has a lower oxidation state than the ULS. So, it can increase more in the same time than the ULS.

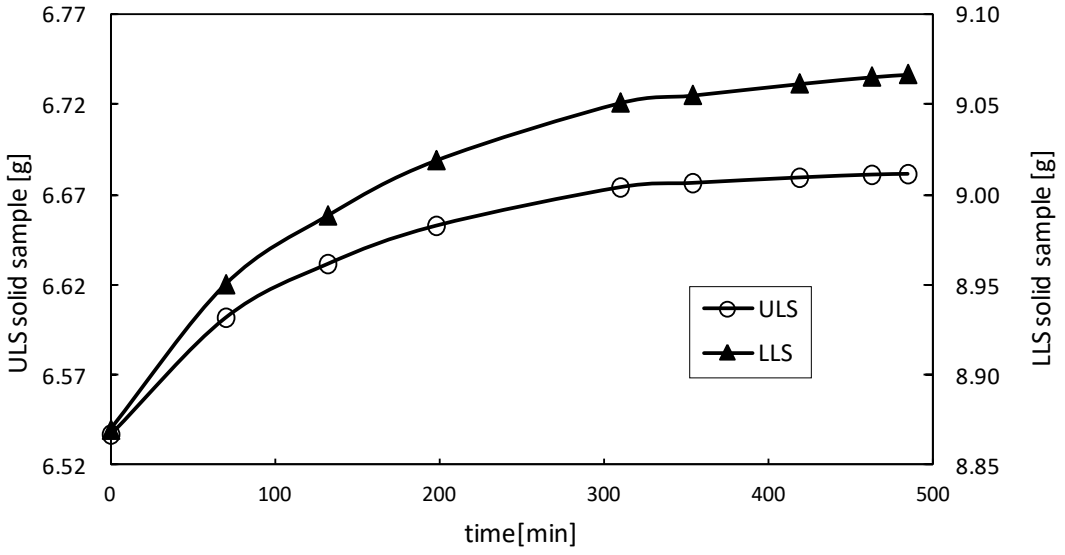

Figure 4. 16: Cu15 OC: increase of the mass of the solid sample [g] over time [min] under ambient conditions (Operating point E)

4.4.1 Determination of R_0 via the reduction furnace

The measurements of the Reduction furnace which is described in section 3.2 is shown in the next tables.

Table 4. 3: Shows the first samples of the reduction furnace.

	TEMPERATURE	REDUCTION TIME	H_2	R_0
UNITY	[°C]	[h]	[%]	[-]
SAMPLE 1.1	900	1	5.20	0.0100
SAMPLE 1.2	900	2	5.20	0.0195
SAMPLE 2.1	900	1	4.60	0.0146
SAMPLE 2.2	900	1	4.75	0.0141
SAMPLE 3.1	900	5	6.00	0.0097
SAMPLE 3.2	900	5	6.39	0.0096

It can be seen in sample 1 that the reduction time is an important parameter. After one hour of reduction (1.1) the calculated oxygen transport capacity (R_0) is much lower than after 2 hours of reduction (1.2) of the same sample amount. The different H_2 values at sample 2.1 and 2.2 show only small changes in the oxygen transport capacity in comparison to the reduction time changes. Therefore, the parameter with the greatest influence on the calculated R_0 is the reduction time. An additional error is that Cu reacts with air in ambient temperatures. Therefore, weighing has to be done as fast as possible under ambient temperature, and there should be as little contact with air as possible. This is shown in section 4.4.

The solid samples which are used for the analysis are shown in Table 4. 4 and Table 4. 5.

Table 4. 4: Parameters of the operating point samples for the sensitivity analysis

	TEMPERATURE	REDUCTION TIME	H_2	R_0
UNITY	[°C]	[h]	[%]	[-]
SAMPLE A	900	1.5	6.20	0.026538
SAMPLE B	900	1.5	6.29	0.027474

The important parameters for the sensitivity analysis are the oxygen transport capacity and the CuO content of the solid sample.

The CuO content is calculated with the reduction equation (16) mentioned in section 3.2. The stoichiometric calculation of this reaction and with the help of the results of the reduction furnace, the CuO content is calculated. The original OpPt were analysed with the XRF (section 3.3) to get the CuO content and subsequently R_0.

The evaluation of some operating points is performed again with values of R_0 obtained from the reduction furnace. The impacts of the changed parameters are compared to the original operating points. Those impacts are shown in the next chapter.

Table 4. 5: Masses and CuO content of the operating point samples for the sensitivity analysis

	SAMPLE MASS	REDUCTION MASS	OXIDATION MASS	CUO CONTENT
UNITY	[g]	[g]	[g]	[%]
SAMPLE A	4.5712	4.5082	4.6311	13.20
SAMPLE B	4.8156	4.7328	4.8665	13.65

4.4.2 Influence of the CuO content on process parameters

The sensitivity analysis of the CuO contents describes the influence of the CuO content on the parameters: global solids circulation rate, the oxygen carrier to fuel ratio and the statistic error. The statistic error summarizes the quality of all measured data. It was done because of the different result of the CuO content of the measurements. Those measurements of the solid samples were the TGA, XRF and the reduction furnace.

Three analyses of the CuO content were done at the *Technischen Universität Wien* and at the Spanish National Research Council (CSIC). CSIC has made the TGA analyses whereas the XRF and the results of the reduction furnace were done at the TUW. For those analyses six operating points (A-F) were chosen to be evaluated.

Table 4. 6 shows those six operating points and their CuO content of the different analytic methods. TGA and reduction furnace analytics are compared to the XRF analytics which are shown below. At OpPt C and D the TGA values were too low, resulting in physically impossible results, i.e. $X_{s,LLS} < 0\%$. So, the lowest possible value is chosen. Those were OpPt C 14.2% and OpPt D 14.4%.

Table 4. 6: Measurements of the Analytics: XRF Data, TGA Data and Reduction Data

OPERATING POINT SAMPLE	XRF-CUO-CONTENT(TUV) [%]	TGA-CUO-CONTENT(CSIC) [%]	REDUCTION FURNACE(TUV) [%]
A	16	10.6	-
B	16	10.3	-
C	16.22	10.3/14.2	-
D	16.6	10.3/14.4	-
E	14	-	13.2
F	14	-	13.65

With these different CuO contents the evaluation via process simulation was reperformed. Those new values replaced the original CuO values. With that information a comparison of the general evaluation to the modified ones with the different CuO contents is possible.

Figure 4. 17 shows a comparison of the different values of CuO contents and their influence on the investigated parameters. It shows that the OpPt A and B have in general the highest differences between the two operating conditions (general evaluation to changed CuO content evaluation). All three parameters, Φ, G_s and the statistic error, change more than for the other OpPts. This is because the CuO content change is the highest when compared to the other four OpPts.

It can be seen that with decreasing CuO content the OC to fuel ratio changes the most. At OpPt A and B the change of the OC to fuel ratio is at nearly -50%. Operating points E and F have the lowest change of the Φ, because of the lowest CuO content deviation. But also at smaller changes of the CuO content the effect on the Φ is visible. At OpPt F the CuO content drops about -2.5% and the oxygen carrier to fuel ratio drops about -3.4%.

After the OC to fuel ratio, the global solid circulation rate is the next parameter with a decrease. The change is much lower than the OC to fuel ratio but also at OpPt A -2.3%. The change of the statistic error has the lowest deviation with a maximum decrease of -0.27% at OpPt E.

That will lead to the assumption that the CuO content has the most impact on the change of the OC to fuel ratio.

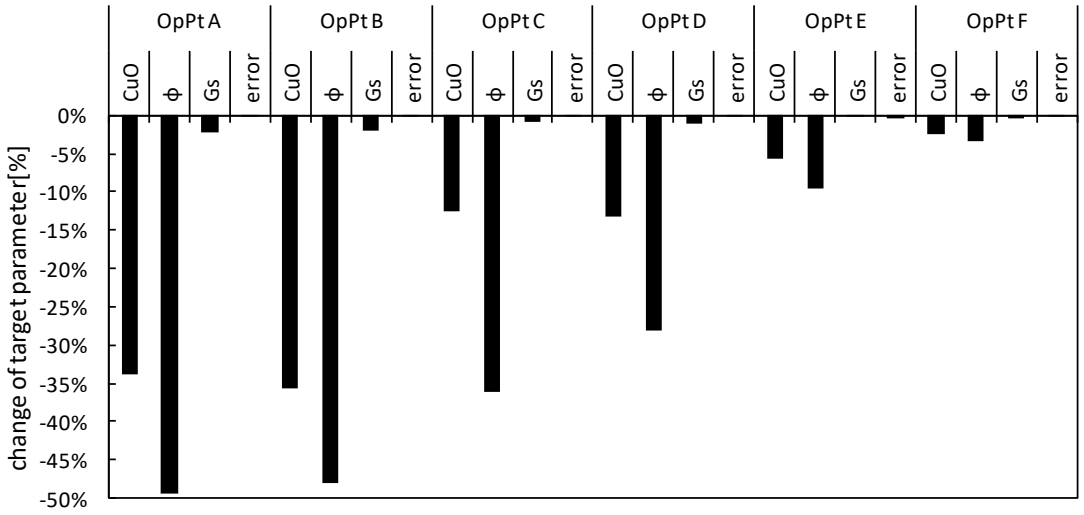

Figure 4. 17: Deviation of the modified point to the operating point

Figure 4. 18 shows the sensitivity parameter, i.e. the variation of the CuO content in relation to the variation of the changed parameters. Therefore, the sensitivity is normalized. It can be seen that the OC to fuel ratio reacts most on the change of the CuO content. That change of the Φ is because of the decrease of the particle oxidation states in the ULS and the LLS. That leads to the conclusion that a lower CuO content results in a bigger ΔX_s.

Compared to the OC to fuel ratio, the other two parameters are negligible. The G_s is <0.1 and the statistic error is nearly zero.

In conclusion it can be said that the change of the CuO content has an influence on the value of the relative oxidation state. Therefore, an error during determination of the CuO content has a big influence on the OC to fuel ratio. An effect on the Global solid circulation rate is present but so low that the results are trustable. The statistic error is not really affected by this change. With respect to these results, the general performance is valid, besides the OC to fuel ratio. Therefore, the Φ is not used in the general performance.

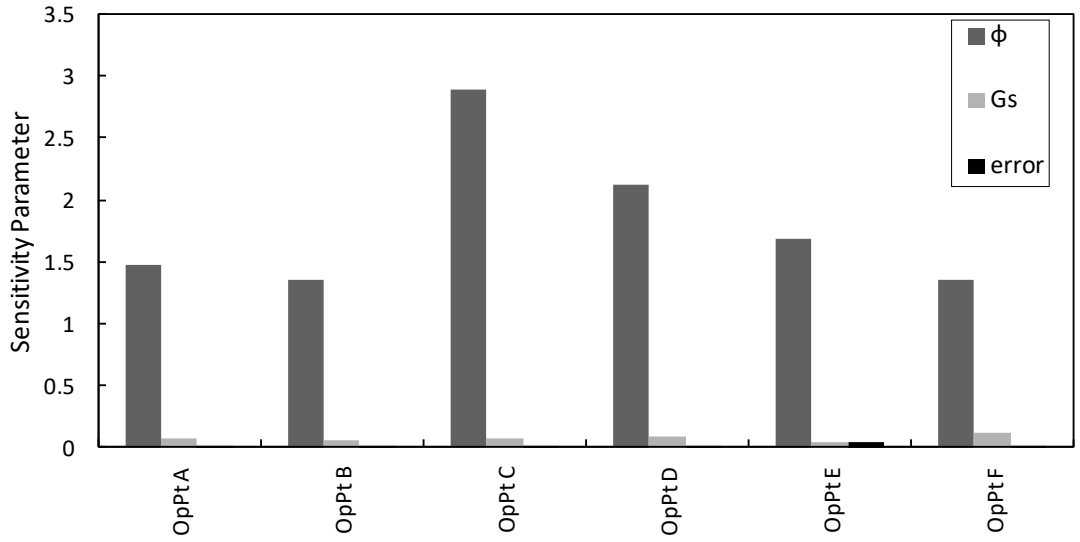

Figure 4. 18: Sensitivity Parameter ξ of all modified OpPt

4.4.3 Influence of the sample weight on process parameters

The second analysis, which was done, analyses the influence of the potential error of the initial weight of the solid sample on the parameters G_s, Φ and the statistic error. The problems which appear during the solid measurement of the oxidation state initiate that analysis. As mentioned in section 4.4 the mass of the solid sample increases over time at ambient temperature and conditions. This could lead to errors in the results of the evaluation of the process. To investigate the influence of the initial weight of the sample, the weight was changed by a certain percentage. The difference, results in a change of the oxidation state of the OpPts. The effect of that change is analysed using the same parameters as in the chapter before: the OC to fuel ratio, the global circulation rate and the statistic error.

The analysed OpPt are the same ones as in the CuO content sensitivity analysis, but the difference is that the initial weight of the solid sample is changed and not the CuO content.

The initial weight of the general evaluation is changed by a certain factor to get the weight with the potential error:

$$m_{M\_OpPt} = m_{OpPt} * f \tag{30}$$

The used value of the factor can be seen in Table 4. 7. Those intervals are used because stronger changes could not be evaluated. This is because in the case of increasing the initial weight, $X_{s,ULS}$ will be higher than 100% and in the case of decreasing, the $X_{s,LLS}$ will be lower zero. Therefore, the difference between the weight with the potential error and the original initial weight is only ±0.4% and ±0.3%. That change will lead to a very small change of the absolute values of the initial weight. For example, for OpPt A the difference is at ±0.4%: ±0.0584g for the ULS and ±0.0255g for the LLS.

Table 4. 7: Changes of the initial sample mass with the factor f

DECREASE OF 0.4%	m_{OpPt} * 0.996
DECREASE OF 0.3%	m_{OpPt} * 0.997
INCREASE OF 0.4%	m_{OpPt} * 1.004
INCREASE OF 0.3%	m_{OpPt} * 1.003

Figure 4. 19 shows how the change of the weight affects the $X_{s,ULS}$. It shows the influence of the error of the initial weight on the oxidation state of each operating point. It can be seen that the error leads at ±0.3% to a change of $X_{s,ULS}$ ±10%, whereas it leads at ±0.4% to a change of $X_{s,ULS}$ ±14%.

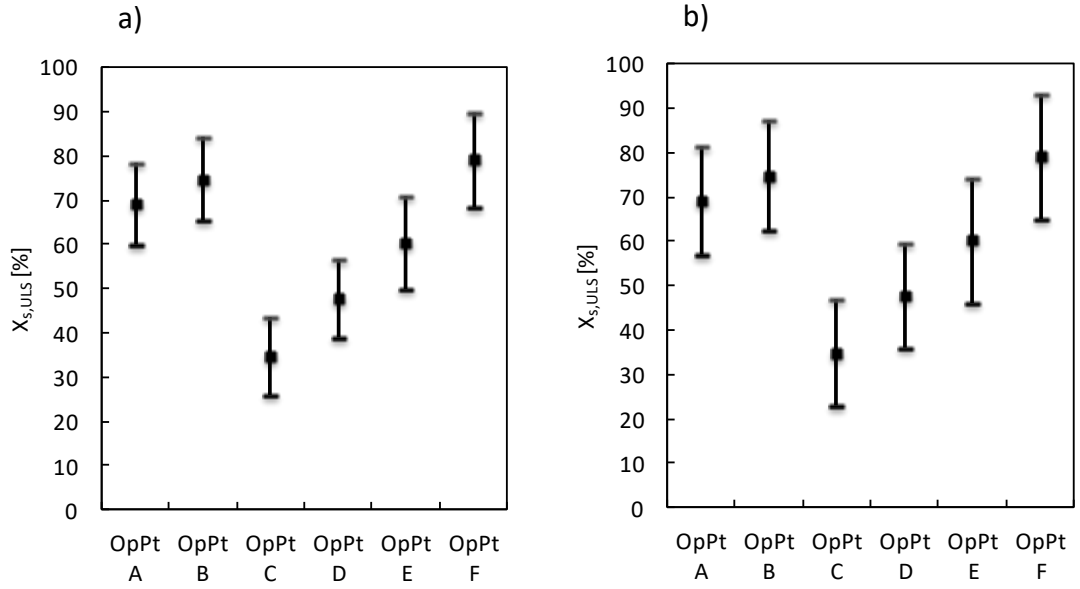

Figure 4. 19: Influence of the initial weight with potential error on the $X_{s,ULS}$ on the example of ±0.3% (a); ±0.4% (b);

The same effect of the weight with the potential error can be seen at the oxidation state of the lower loop seal. Figure 4. 20 shows the same changes of the oxidation state as mentioned before at the $X_{s,ULS}$.

Those differences have an influence on the evaluation. The effects on the three analysed parameters will be explained in the next pages.

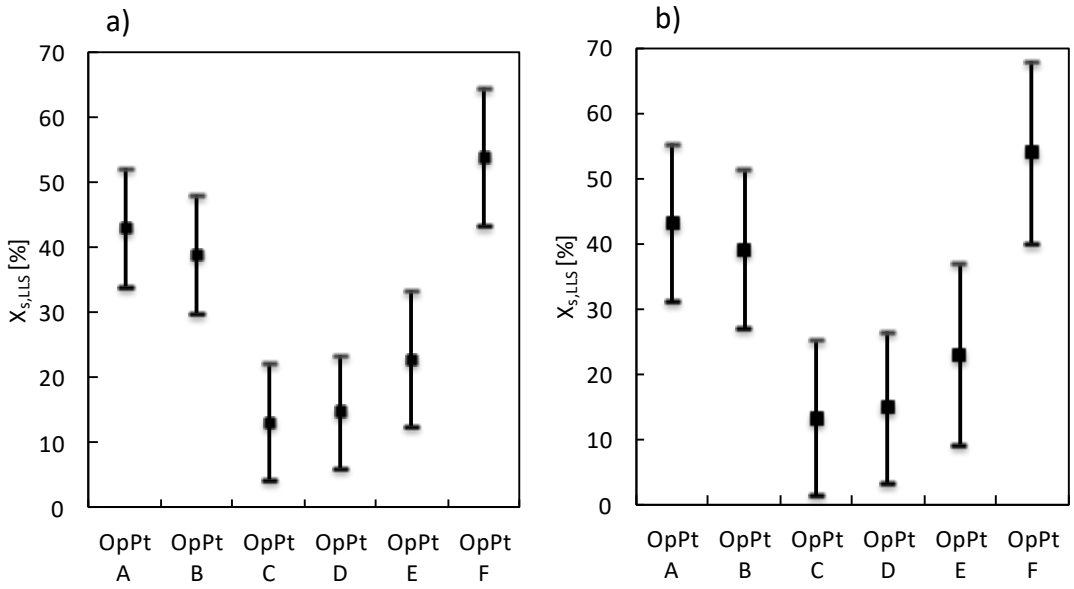

Figure 4. 20: Influence of the initial weight with potential error on the $X_{s,LLS}$ on the example of ±0.3% (a); ±0.4% (b)

The influence of the potential error of the initial weight on the OC to fuel ratio is significant. In Figure 4. 21 the evaluation of the Φ after the changed weight can be seen. Considering each operating point and their changed results individually, a linear behaviour can be seen. For example, an increase or decrease by 0.4% of the solid sample mass lead to a change of the OC to fuel ratio by ±34%. The reason is that the particle oxidation state increases with the mass increase, because the CuO content is constant.

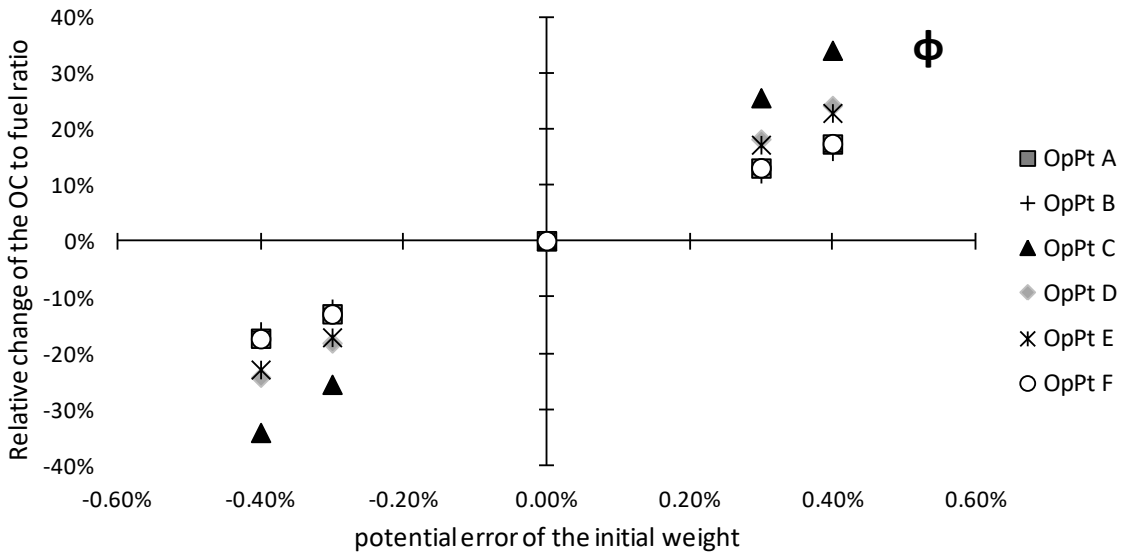

Figure 4. 21: Effect of oxygen carrier to fuel ratio at different solid sample masses

Generally, the change of the initial weight of the solid sample has the greatest impact on the OC to fuel ratio. With the same change of weight, the global solid circulation rate and the statistic error were compared to the original operating point.

The relative change of the G_s and the statistic error is much lower than the OC to fuel ratio. That can be seen in Figure 4. 22 and Figure 4. 23. The two parameters do not change more than ±0.2% to the original operating point.

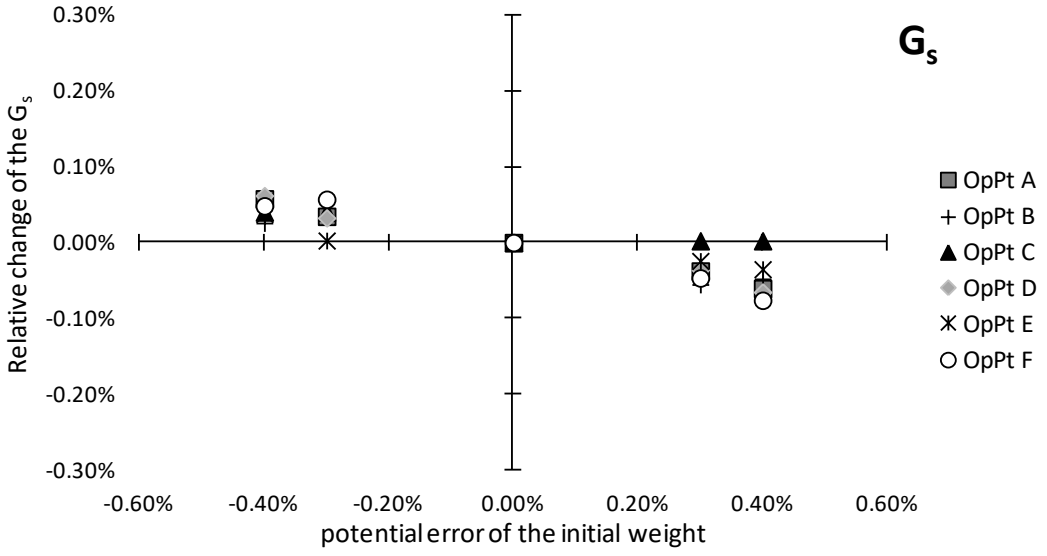

Figure 4. 22: Effect of global solid circulation rate at different solid sample masses

The influence of the potential error on the initial weight has the lowest influence on the Global circulation rate. These do not even exceed ±0.1%. This can be seen in Figure 4. 22.

The changing mass also exhibits a negligible influence on the statistic error (Figure 4. 23). All operating points are lower than ±0.1%, but OpPt E and F are a little bit higher. A possible reason of this is that a change of the oxidation state at both points is much more than at the other ones. Both OpPt $X_{s,ULS}$ are higher than ±14%, whereas the others have ±12%.

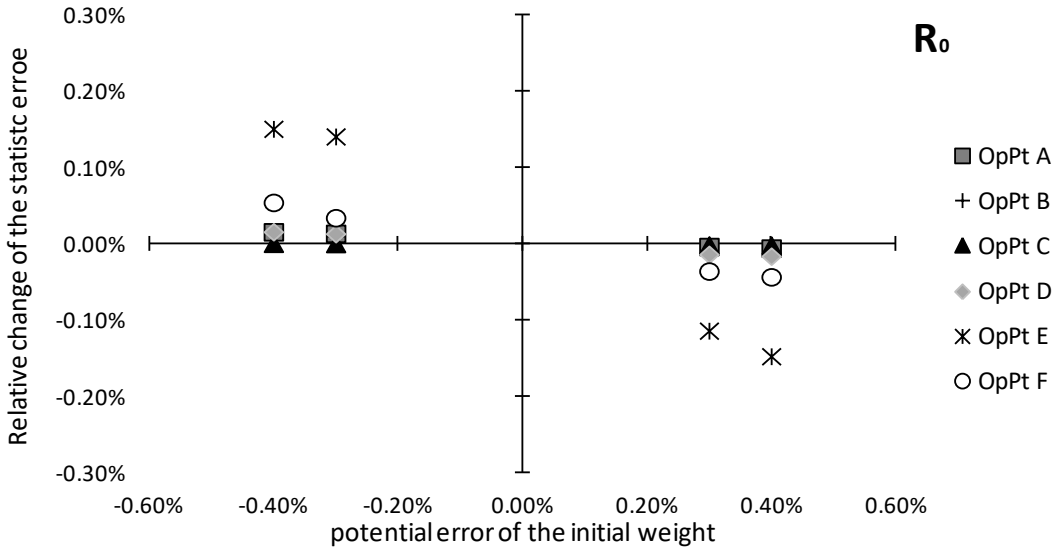

Figure 4. 23: Effect of statistic error at different solid sample masses

In conclusion the potential error on the initial weight has a great effect on the OC to fuel ratio. Therefore, the Φ does not provide reliable information on the performance. Besides Φ, the G_s and the statistic error have no effect because of the potential error of the initial weight.

General it can be said, that a change of the oxidation state has an impact on the process performance. Therefore, the investigations on different parameters were done, which were affected by the oxidation state.

Therefore, as general conclusion of the sensitivity analysis, it can be said that the CuO content change as well as the potential error of the initial weight had the greatest influence on the OC to fuel ratio. Especially the potential error of the initial weight is more significant and problematic compared to the CuO content. This is because much smaller changes to the reference parameter of the sample weight have greater effects on the resulting parameters than is the case of a wrong CuO content.

But besides those significant results the essence information obtained about the operating points and their resulting measurements is that they are accurate and credible, regarding solid circulation rate. That means that the overall message of the performance is right. Only the OC to fuel ratio is not credible and is therefore not used in the general performance evaluation.

5. CONCLUSION AND OUTLOOK

This thesis was performed to evaluate oxygen carrier for chemical looping combustion. The oxygen carrier is a copper-based material which is an impregnation of a CuO on an Al_2O_3 support material. The experiments were done at the *Technischen Universität Wien* on a 120kW pilot rig. This pilot plant works with a Dual Fluidized Bed System (DCFB), where the air and fuel reactor are separated and connected with loop seals. During the experiments gas analytics and after the experiments solid analytics of the operating points were done. The raw data of each operating point during the experiments were validated and uploaded using the process simulation program IPSEpro of *Simtech simulation technology*.

A copper-based OC, CuO/Al_2O_3, was previously investigated at the *Technischen Universität Wien* in 2013 and was the benchmark for this thesis. Furthermore, copper-based oxygen carriers were also tested in smaller units like 500W or 10kW units.

During the experiments different parameters were investigated like temperature, air to fuel ratio, fuel power or inventory. Additional to those parameters, other fuels were added to the standard fuel. Apart from natural gas, propane and pentane were also used. Those higher hydrocarbons were also analysed on performance and conversion.

Besides the online gas analytics, solid samples were taken during all experiments. Those samples of the Cu15 material were also analysed with a reduction furnace just as TGA and XRF. Those different values, of the CuO content, of the three analyses were taken to find out their effects on the process. Additional to the CuO content change, the error of the initial weight was also analysed. It was analysed because of uncertainties by the evaluation of the weight of the sample. Therefore, a sensitivity analysis and their influence on the oxidation state were done by using different initial weights and CuO contents of the oxygen carrier material.

5.1 The results of the general performance of the Cu15 oxygen carrier

Fuel power, specific inventory:

The results of the variation of fuel power between 50kW and 90kW concluded that a lower fuel power leads to a lower residence time of the solid in the FR. This results in a longer contact between particles and fuel and therefore to a better fuel conversion. Additional to that a higher specific inventory in the FR leads therefore also to a better

fuel conversion. More inventory in the FR leads to a possibility of higher contact between the gas and solid materials. The consequence is that higher inventory in the FR leads to a higher methane conversion and a higher carbon dioxide yield and in conclusion to a better performance because more O_2 is available.

Temperature:

The influence of the temperature on the methane conversion increases nearly linear. Therefore, the performance of the Cu15 material increases with higher temperatures. At 900°C full conversion was possible and no CO, H_2 or CH_4 was detected in the FR exhaust gas.

Air to fuel ratio:

A tendency of the influence of the air to fuel ratio, λ, on the performance cannot be seen. The oxidation state in the upper loop seal shows constant behaviour, which could be interpreted that the air reactor is limited, but this has to be taken carefully because of measuring errors of the oxidation state (sensitivity analysis). Only a longer residence time of the solid in the AR shows a tendency of a better methane conversion.

Solid circulation, OC to fuel ratio:

With a higher global circulation rate, G_s, the methane conversion increases too. This can be also explained with the higher active inventory in the air reactor and therefore with the higher available oxygen in the fuel reactor.

It was able to calculate the oxygen carrier to fuel ratio, but with the measuring error of the oxidation state, it is not credible and therefore not shown in this thesis. That error and their effects are shown in the sensitivity analysis.

Higher hydrocarbons:

No complete conversion was possible for any mixtures. Mainly CH_4 and nearly no higher hydrocarbons were detected in the FR exhaust gas stream. The lowest CO_2 yield was measured at the mixture of all three species of fuels. Additionally it can be seen that at lower FR specific inventories, the higher hydrogen mixtures showed better combustion efficiency than the pure natural gas operating points. At higher specific inventories in the FR, the combustion efficiency is nearly the same.

Material loss and elutriation:

During the CLC process, the OC is under permanent stress, which can be mechanical-, thermal- and chemical stress. At the beginning of every experiment, elutriation of fine particle can be seen. After that, the material loss during the experiment was nearly constant.

Influence of the measurement errors on process parameters:

The two sensitivity analysis based on the potential error of the initial weight and the different results of the measurements of the CuO content. Those two changes of the masses and the CuO content have an influence on the oxidation state of the solid sample. In both cases the CuO content changes as well as the potential error of the initial weight had the greatest influence on the oxygen carrier to fuel ratio. That result supported that the oxygen carrier to fuel ratio is not credible and therefore not used in this thesis.

The other two analysed parameters, the statistic error and the global solid circulation rate, had much lower effects of the change of the CuO content or the potential error of the initial weight. That implied that those parameters are credible and used to analyse the performance of the process.

5.2 Outlook

- The general performance of the process was good and the results of the thesis should be taken to analyse some topics more in detail. One of them is the air to fuel ratio. The result is not significant and should be investigated further.
  The determination of the oxidation state causes also problems. This measurement procedure must be improved to reach a better and an optimized process.

- A higher temperature improves the performance of the chemical looping process. Besides those results an economic analysis of the resulted cost and optimal conditions should be done. The raising cost are the higher amount of the oxygen carrier itself, because of the higher stress on the oxygen carrier, and the higher energy demand, because of the higher temperatures.

- Another aspect is to investigate the process with contaminations. Those contaminations are for example sulphur or nitrogen compounds and appear in different fuels and in different concentrations. To know how the contamination will influence the efficiency of the process, this should be also investigated.

- The inventories in the reactors are one of the main driver to raise the process performance. Therefore, the reactors should contain more solid amount which leads to a larger scale of plant.

6. ABBREVIATIONS

AET-Lib	Advanced Energy Technology library
AFOLU	Agriculture, Forestry and Other Land Use
AR	Air reactor
BECCS	bio-energy with CCS
CCU	Carbon capture and utilisation
CCS	Carbon Capture and Storage
CLC	Chemical looping combustion
CSIC	Spanish National Research Council
CLOU	Chemical looping with oxygen uncoupling
Cu15	Copper based oxygen carrier
C28	Mn based oxygen carrier
DCFB	Dual circulating fluidized bed
EOR	Enhanced Oil Recovery
FR	Fuel reactor
FTB	Fire tube burner
GC	Gas chromatography
GHG	Green house gas
HHC	Higher hydrocarbons
IEA	International Energy Agency
IGCC	Integrated gasification combined cycle
ILS	Internal loop seal
IPCC	Intergovernmental Panel on Climate Change
IPSEpro	Integrated Process Simulation Environment
LHV	Lower heating value
LLS	Lower loop seal
MeO	metal oxide
Ng	Natural gas

OC	Oxygen carrier
OpPt	Operating point
PCC	Post Combustion Capture
RCP	representative concentration pathways
Syngas	synthesis gas
TGA	Thermo gravimetric analysis
TUW	Technische Universität Wien
ULS	Upper loop seal
UNFCCC	United Nations Framework Convention on Climate Change
XRF	X-ray fluorescents analysis

7. SYMBOLS AND NOTATION

Ar	Archimedes number	-
A	surface	m^2
b	stoichiometric coefficient	-
C	gas concentration	mol/m^3
d_p^*	dimensionless particle diameter	-
d_p	particle diameter	m
Fr	Frode Number	-
g	Gravitational constant	m/s^2
G_s	Global solid circulation rate	kg/m^2s
m	mass	kg; g
$\dot{m}$	mass flow	kg/s
$\dot{n}$	Molar flow	mol/s
U^*	dimensionless gas velocity	-
U_{mb}	minimum bubbling velocity	m/s
U_{mf}	minimum fluidization velocity	m/s
U_c	critical gas velocity	m/s
U_{se}	solids entrainment velocity	m/s
Re	Reynolds Number	-
R_0	Oxygen transport capacity	%
T_{Fr}	FR Temperature	°C
P	fuel power	kW
Δp	pressure difference	bar
ρ_g	Destiny gas	kg/m^3
Δρ	destiny difference	kg/m^3
μ	Dynamic Viscosity	kg/ms
X_i	species i; chemical conversion	mol/mol
X_s	particle oxidation state	%

Y_i	Yield i	mol/mol
λ	air to fuel ratio	-
ϕ	oxygen carrier to fuel ratio	-
ξ	sensitivity parameter	-

8. REFERENCES

[1] B. Obama, “Inaugural Address by President Barack Obama,” The White House; Office of the Press Secretary, 21 January 2013. [Online]. Available: https://obamawhitehouse.archives.gov/the-press-office/2013/01/21/inaugural-address-president-barack-obama. [Accessed 17 04 2017].

[2] O. Edenhofer, R. Pichs-Madruga, Y. Sokona, E. Farahan, S. Kadner, K. Seyboth, A. Adler, I. Baum, S. Brunner, P. Eickemeier, B. Kriemann, J. Savolainen, S. Schlömer, C. von Stechow, T. Zwicjel and J. Minx, “IPCC, 2014: Climate Change 2014: Mitigation of Climate Change. Contribution of Working Group III to the Fifth Assessment Report of the Intergovernmental Panel on Climate Change,” Cambridge University Press, Cambridge, United Kingdom and New York, NY, USA, 2014.

[3] E. Wolff, I. Fung, B. Hoskins, J. Mitchell, T. Palmer, B. Santer, J. Shepherd, K. Shine, S. Solomon, K. Trenberth, J. Walsh and D. Wuebbles, Climate Change Evidence & Causes: An overview from the Royal Siciety and the US National Acedamy of Siences, National Acedamy of Sience, The Royal Society.

[4] S. Penthor, Dissertation: Chemical Looping Combustion of Biomass for below zero emission energy production, Wien: Technical university of Vienna, 2015, pp. 15 - 20.

[5] I. E. A. (IEA), “Carbon Capture and Storage: The solution for deep emissions reductions,” IEA Publications, France, 2015.

[6] R. M. Cuellar-Franca and A. Azapagic, Carbon capture, storage and utilisation technologies: A critical analysis and comparison of their life cycle environmental impacts, vol. 6, Manchester: Journal of CO2 Utilization, 2015, pp. 82 - 102.

[7] M. Stollhof, Detailed fluid dynamic investigations of the fuel reactor of a novel DUAL, FLUID reactor concept for Chemical Looping Combustion for solid fuels, Wien: Technische Universität Wien, 2014.

[8] D. Dürr, “Carbon Capture and Storage (CCS) Chance und Risiken der Kohlendioxidabscheidung und -speicherung,” Inagendo GmbH, Ahrstraße 1, D-53859 Niederkassel, 2009.

[9] H. Hofbauer, Unterlagen zur Vorlesung: Wirbelschichttechnik 159.220, vol. 6. Auflage, Wien: Technical Universitiy of Vienna Eigenverlag, 2013, pp. 2 - 31.

[10] D. Geldart, Types of Gas Fluidization Power technology 7, Lausanne, printed in the Netherlands: Elsevier Sequoia S.A., 1973, pp. 285 - 292.

[11] J. M. V. Millan, Fluidization of fine Powders, vol. Volume 18, Netherlands: Springer Netherlands, 2013, p. 2.

[12] H. T. Bi and J. R. Grace, "Flow Regime Diagrams for Gas - Solid Fluidization and upward Transport," Elsevier Science Ltd, Great Britain, 1995.

[13] J. R. Grace, A. A. Avidan and T. M. Knowlton, Circulating Fluidized Beds, London, UK: Published by Blackie Acadamic and Professional, an imprint of Chapman & Hall, 1997, pp. 6 - 12.

[14] T. Pröll, Habilitationsschrift: Innovative Fuel Conversion with CO2 Capture Using Dual Fluidized Bed Systems, Wien: Technical University of Vienna, 2011.

[15] E. R. Gilliland and W. K. Lewis, "Porduction of pure carbon dioxide". USA Patent US 2665972 A, 12 Jan 1954.

[16] P. Kolbitsch, Dissertation: Chemical Looping combustion for 100% carbon capture - Design, operation and modeling od a 120kW pilot rig, Wien: Technical University of Vienna, 2009, pp. 16 - 19, 30 - 34.

[17] A. Lyngfelt, B. Leckner and T. Mattisson, A fluidized - bed combustion process with inherent CO2 separation; application of chemical - looping combustion, vol. 56, Göteborg, Sweden: Chemical Engerneering Science, 2011, pp. 3101 - 3113.

[18] M. Abbasi, M. Farniei, M. R. Rahimpour and A. Shariati, Hydrogen Production in an Environmental - Friendly Process by Application of Chemical Looping Combustion via Ni - and Fe - Based Oxygen Carriers, vol. 49, Iran: Theoretical Foundations of Chemical Engineering, 2015, pp. 884 - 900.

[19] M. Arjmand, A.-M. Azad, H. Leion, A. Lyngfelt and T. Mattisson, Prospects of Al2O3 and MgAl2O4 - Supported CuO Oxygen Carriers in Chemical - Looping Combustion (CLC) and Chemical-Looping with Oxygen Uncoupling (CLOU), vol. 25, Goeteborg, Sweden: Energy & Fuels, 2011, pp. 5493 - 5502.

[20] K. Mayer, Diplomarbeit: Ilmenite and mixtures with Olivine as oxygen carriers in a chemical looping combustion pilot plant, Wien: Technische Universität Wien, 2010, pp. 41 - 46.

[21] P. Kolbritsch, T. Pröll and H. Hofbauer, Modeling of a 120kW chemical looping combustion reactor system using Ni-based oxygen carrier, vol. 64 (1), Vienna:

Chemical Engineering Science, 2009, pp. 99 - 108.

[22] J. Adanez, P. Gayan, J. Celaya, L. F. de Diego, F. Garcia-Labiano and A. Abad, Chemical Looping Combustion in a 10 kWth Prototype Using a CuO/Al2O3 Oxygen Carrier: Effect of Operating Conditions on Methane Combustion, vol. 45, Zaragoza, Spain: Ind. Eng. Chem. Res., 2006, pp. 6075 - 6080.

[23] A. Cabello, P. Gayan, A. Abad, d. Diego, F. Garcia-Labiano, M. Izquierdo, A. Scullard, G. Williams and J. Adanez, Long - lasting Cu - based oxygen carrier material for industrial scale in Chemical Looping Combustion, vol. 52, Saragossa, Spain: International Journal of Greenhouse Gas Control, 2016, pp. 120 - 129.

[24] F. Zerobin, Master Thesis: Evaluation of a CuO/Al2O3 oxygen carrier for Chemical Looping Combustion, Wien: Technical University of Vienna, 2013.

[25] L. F. de Diego, P. Gayan, F. Garcia-Labiano, J. Celaya, A. Abad and J. Adanez, Impregnated CuO/Al2O3 Oxygen Carriers for Chemical - Looping Combustion: Avoiding Fluidized Bed Agglomeration, Zaragoza, Spain: Energy & Fuels, 2005, pp. 1850 - 1856.

[26] S. Penthor, F. Zerobin, K. Mayer, T. Pröll and H. Hofbauer, Investigation of the performance of a copper based oxygen carrier for chemical looping combustion in a 120 kW pilot plant for gaseous fuels, vol. 145, Vienna, Austria: Applied Energy, 2015, pp. 52 - 59.

[27] A. Lyngfelt, Oxygen Carriers for Chemical Looping Combustion - 4 000 h of Operational Experience, Vols. 66, 2, Oil & Gas Science and Technology – Rev. IFP Energies nouvelles, 2011, pp. 161 - 172.

[28] T. Pröll, P. Kolbitsch, J. Bolhar-Nordenkampf and H. Hofbauer, Chemical Looping Pilot Plant Results Using a Nickel-Based Oxygen Carrier, Vols. 66, No 2, Vienna: Oil & Gas Science and Technology – Rev. IFP Energies nouvelles, 2011, pp. 173-180.

[29] K. Mayer and e. at., The different demands of oxygen carriers on the reactor system of a CLC plant – Results of oxygen carrier testing in a 120kWth pilot plant, Vienna: Applied Energy, 2015.